Progress in Oceanography 231 (2025) 103388

Contents lists available at ScienceDirect

Progress in Oceanography

journal homepage: www.elsevier.com/locate/pocean

A predictive krill distribution model for *Euphausia pacifica* and *Thysanoessa spinifera* using scaled acoustic backscatter in the Northern California Current

S. Derville [a,b,*], J.L. Fisher [c], R.L. Kaplan [a,d], K.S. Bernard [d], E.M. Phillips [e], L.G. Torres [a]

[a] *Geospatial Ecology of Marine Megafauna Lab, Marine Mammal Institute, Department of Fisheries, Wildlife and Conservation Sciences, Oregon State University, Newport, OR, United States*
[b] *UMR ENTROPIE (UR-IRD-IFREMER-CNRS-UNC), Nouméa, New Caledonia*[1]
[c] *Fish Ecology Division, Northwest Fisheries Science Center, National Oceanic and Atmospheric Administration, Newport, OR, Unites States*
[d] *College of Earth, Ocean, and Atmospheric Sciences, Oregon State University, Corvallis, OR, United States*
[e] *Fishery Resource Analysis and Monitoring Division, Northwest Fisheries Science Center, National Oceanic and Atmospheric Administration, Seattle, WA, United States*

ARTICLE INFO

Keywords:
Krill
Hydroacoustics
Net tow
Species distribution models
Shelf break
Upwelling
Predictions

ABSTRACT

Euphausiids (krill) are globally significant zooplankton prey for many commercially important or endangered predator species. In the productive upwelling system of the Northern California Current (NCC), two krill species, *Euphausia pacifica* and *Thysanoessa spinifera,* dominate the preyscape and constitute an important food resource for many seabirds, cetaceans, and fish. In this study, we use five years of hydroacoustic and net tow data collected in the NCC to develop integrative models predicting acoustic backscatter scaled for *E. pacifica* or *T. spinifera* separately. Boosted Regression Trees and Generalized Additive Models are applied in an original ensemble hurdle framework to predict krill presence and abundance from a diverse set of topographic and oceanographic predictors. Krill metrics had significant relationships with seabed depth, distance to submarine canyons, and variables indicative of dynamic ocean conditions (e.g., total deviance explained in acoustic data: 25 % in the presence-absence model & 49 % in the abundance model). Predictions of krill abundance at 5 km resolution averaged by month indicate differential habitat preferences between the two species: *T. spinifera* was constrained to the continental shelf, around and inshore of the 200 m isobath, whereas *E. pacifica* was found in greater abundances just offshore of the 200 m isobath and into offshore water in lower abundances. *E. pacifica* was generally more abundant than *T. spinifera* (10:1.3 ratio). Both species increased in abundance in the spring and summer, followed by a rapid decline in the fall, and lowest abundances in the winter. These models can produce fine-scale spatial and year-round weekly predictions of *E. pacifica* and *T. spinifera* abundance in the NCC, which will provide essential knowledge and new spatial layers about critical ecosystem components to support research and management.

1. Introduction

Zooplankton play essential roles in global marine biogeochemical cycles (Tovar-Sanchez et al., 2007) and pelagic food webs as they form an important link between primary producers and higher trophic levels in the ocean (Ruzicka et al., 2012). Understanding the habitat and environmental drivers of zooplankton spatiotemporal dynamics is essential for predicting the pelagic ecosystem's response to climate change (Ratnarajah et al., 2023). In particular, improved knowledge of variation in zooplankton distribution is needed to enhance estimates of predator distributions and trends in managed fish stocks within a changing and increasingly anthropized ocean.

Euphausiids, hereafter "krill", are important zooplankton prey in the California Current, an eastern boundary current flowing equatorward along the North American west coast (Checkley and Barth, 2009). In this highly productive ecosystem, krill are consumed by a variety of predators, including marine mammal and seabird species (e.g., blue whales, *Balaenoptera musculus*, and humpback whales, *Megaptera novaeangliae,*

* Corresponding author.
E-mail address: solene.derville@ird.fr (S. Derville).
[1] (present address).

https://doi.org/10.1016/j.pocean.2024.103388
Received 2 July 2024; Received in revised form 24 September 2024; Accepted 25 November 2024
Available online 27 November 2024

Fossette et al., 2017; Cassin's Aucklets, *Ptychoramphus aleuticus*, Abraham and Sydeman, 2006, 2004; Ainley et al., 1996; Sydeman et al., 1997; Sooty shearwaters, *Puffinus griseus*, Chu, 1984; Santora et al., 2012) and fish species of economic significance (Hill et al., 2015), including anchovies (*Engraulis mordax*, Brodeur et al., 1987), Pacific sardines (*Sardinops sagax*, Emmett et al., 2005; Hand and Berner, 1959), Chinook and Coho salmon (Brodeur et al., 1987; Sabal et al., 2020; Thayer et al., 2014), Pacific hake (*Merluccius productus*, (Bizzarro et al., 2017; Buckley and Livingston, 1997), and several species of rockfish (Lee and Sampson, 2009). Several studies investigated the co-occurrence patterns of krill and their predators in the California Current (Bliss et al., 2024; Cimino et al., 2020; Croll et al., 2005; Kaplan et al., 2024; Phillips et al., 2023; Rockwood et al., 2020; Santora et al., 2012, Santora et al., 2011) and emphasized the value of ecosystem approaches to inform management of essential habitats for both predators and prey. However, krill data is seldom available at the appropriate spatio-temporal scale for inclusion in predator distribution models (Derville et al., 2022). As a result, these models often rely on proxy relationships with environmental predictors due to the absence of prey data (Redfern et al., 2006).

In the California Current, two krill species are dominant: (1) *Euphausia pacifica*, which is the more abundant but smaller-sized species compared to (2) *Thysanoessa spinifera* that is a more energetically profitable species to predators due to their larger body size and higher lipid density (Fisher et al., 2020). The two species overlap in range (Brinton, 1962) and their abundance has been linked to seabed topographic features such as submarine canyons (Santora et al., 2018) and the continental shelf break, delineated by the 200 m isobath (Rockwood et al., 2020; Santora et al., 2011). These two krill species also show distinct habitat preferences in terms of seabed depth: *T. spinifera* tends to occur over the continental shelf (bottom depth ~ 0–200 m), while *E. pacifica* also expands to the shelf break (~ 200 m), the continental slope (~ 200–500 m; as defined in Phillips et al., 2022), and the outer-shelf (> 500 m); Brinton, 1962; Cimino et al., 2020; Dorman et al., 2023; Gómez-Gutiérrez et al., 2005; Santora et al., 2012). As predators are known to adapt their distribution and behavior based on prey availability (e.g., humpback whales, Fleming et al., 2016), and to select specific prey species based on energetic content (e.g., blue whales target *T. spinifera*, Nickels et al., 2018), understanding the spatiotemporal distribution patterns of these two krill species with seasonally varying lipid densities (Fisher et al., 2020) may provide greater insights into the predator distributions and locations and times of the year where lipid-rich prey may be encountered.

Krill distributions are inherently patchy and dynamic both spatially and temporally (Benoit-Bird et al., 2019). They form discrete aggregations and undergo diel vertical migration (Bollens et al., 1992; Brinton, 1967, 1962), a behavior that balances predator avoidance at depth during the day and access to foraging opportunities near the productive surface mixed layer at night. While krill abundance was shown to peak a few months after the onset of seasonal wind-driven upwelling (July-October in Monterey Bay, Croll et al., 2005), their spatial distribution is dissociated from upwelling centers where strong currents occur, and associated instead with retention zones where krill, and presumably their phytoplankton prey, are retained by eddies and slower currents (Dorman et al., 2015b; Santora et al., 2011). Indeed, variable oceanographic conditions are important drivers of local krill abundance (Fiechter et al., 2020). Krill reproductive development, cross-shore and alongshore distribution, and biomass varies in response to basin-scale climatic oscillations, such as the Pacific Decadal Oscillation (PDO) and the El Niño Southern Oscillation (ENSO; Brinton and Townsend, 2003; Peterson et al., 2017; Santora et al., 2017). During negative (cool) phases of the PDO, *T. spinifera* are more abundant and found closer to shore compared to positive phases of the PDO (Shaw et al., unpublished data). Warmer conditions found during El Niño years, positive PDO phases, and extreme marine heatwaves also result in lower krill abundance and biomass (Brinton and Townsend, 2003; Peterson et al., 2017). For example, *E. pacifica* and *T. spinifera* individuals were significantly smaller during the 2014–2016 Northeast Pacific marine heatwave (Killeen et al., 2022; Robertson and Bjorkstedt, 2020). Therefore, understanding how the distribution and abundance of these important prey species varies seasonally, inter-annually, and in relation to environmental variability is needed to inform predictions of the impact of environmental change on higher trophic levels.

The importance of krill in the California Current ecosystem has driven many efforts to quantify variation in their alongshore and interannual abundance patterns, and to relate this variation to environmental conditions (Cimino et al., 2020; Dorman et al., 2015a; Phillips et al., 2022; Rockwood et al., 2020; Santora et al., 2012, 2011). These modeling efforts often capitalize on continuous underway active hydroacoustic data that can provide estimates of krill abundance within the water column over large spatial areas during routine fisheries surveys (e.g., Phillips et al., 2022; Rockwood et al., 2020; Santora et al., 2011). While these acoustic methods allow quantification of krill abundance over much larger spatial areas, and often throughout deeper water depths, than traditional net sampling, they are often unable to discriminate species-specific acoustic signals due to the overlapping frequency response of *E. pacifica* and *T. spinifera*. Given the distinct distribution patterns and energetic quality between these krill species, there are important ecological insights to be gained by separating these two species in quantitative models. For example, Cimino et al., (2020) found that species-specific krill abundance predictions of *E. pacifica* and *T. spinifera* based on catch per unit of effort from net hauls outperformed the combined species krill model, emphasizing the importance of separating these species and modeling their distributions independently in relation to environmental drivers. More recently, Dorman et al., (2023) modeled the distribution of *E. pacifica* and *T. spinifera* from net samples relative to bathymetry to estimate the proportion of the backscatter attributable to each species and investigated temporal variation in species-specific biomass in the central California Current. These species-specific approaches provide promising avenues to more accurately assess the distribution and availability of bioenergetics available to higher trophic levels.

In this study, we expand upon and innovate from prior predictive krill models to assess year-round distribution patterns of *E. pacifica* and *T. spinifera* in the Northern California Current (NCC) from both hydroacoustic and net tow data. Past modelling efforts with a spatio-temporal predictive aim utilized krill data collected in central California and during spring (Cimino et al., 2020), which limits robust extrapolation to other seasons and regions of the California Current. Here, we predict species-scaled acoustic backscatter (Nautical Area Scattering Coefficient, NASC) using five years of *in situ* hydroacoustic and plankton net tow data collected in the NCC over 10 degrees of latitude. Krill presence/absence and abundance or biomass of krill are modeled separately with a hurdle modeling framework that is suited for zero-inflated data (Cragg, 1971). Hurdle models are two-part models that first model the probability of observing a zero, then model the probability of the non-zero positive values. Our framework incorporates best practices in species distribution modeling, including careful choice of topographic and dynamic environmental predictors, use of two different statistical algorithms recognized for their predictive performance (Generalized Additive Models, GAMs; and Boosted Regression Trees, BRTs), blocked cross-validation, and validation of predictions with an external dataset. This comprehensive and integrative framework is described in detail to allow reproducibility and application to other regions and prey species that can be detected through hydroacoustics and captured in nets. We calculate multiple evaluation metrics to assess model performance. We inspect predictions to evaluate three paradigms of krill distribution in the NCC in the current literature: 1) Do monthly predictions follow a seasonal trend of increased abundance (using NASC as a proxy) or biomass after the onset of the upwelling season? 2) Do average spatial predictions show a general association of krill with the continental shelf, shelf break, and slope? and, 3) Is *T. spinifera* predicted to be less abundant and more restricted to the continental shelf compared to *E. pacifica*?

Upon validation of our models through answers to these questions, our fine-scale and year-round weekly predictions of *E. pacifica* and *T. spinifera* species-scaled NASC will provide ecological insight and an important tool for scientists and managers of the NCC region to enhance assessments of the distribution of commercially important or endangered predator species.

2. Material and methods

2.1. Study area and period

Krill hydroacoustics data and net tow samples were collected during 10 research surveys between 2018 and 2022 (hereafter "NCC surveys") conducted in the NCC aboard the NOAA Ship *Bell M. Shimada* (Table S1). These surveys were conducted in February, May, and September, along east–west transects and transits between La Push, WA to Crescent City, Trinidad, or San Francisco, CA, USA, covering the continental shelf, shelf break and slope along each transect, extending up to 200 nautical miles offshore of Newport, OR and 150 nautical miles offshore of Crescent City, CA (Fig. 1).

2.2. Krill data

2.2.1. Hydroacoustic data

Hydroacoustic data were collected via hull-mounted downward-looking Simrad EK60 (2018) and EK80 (2019–2022) narrow-band split-beam echosounders operating at multiple frequencies (18, 38, 70, 120, and 200 kHz). Data were processed using Echoview version 13.1 (Echoview Pty Ltd, Hobart, Australia) following the workflow described by Kaplan et al. (2024) modified after Phillips et al., (2022). All processing steps, including background noise removal, seafloor correction, and krill classification using db-differencing are described in detail in Kaplan et al. (2024). Acoustic data classified as krill were exported as integrated area backscatter (nautical-area-backscattering coefficient, s_A or NASC, $m^2\ nmi^{-2}$) in 10 x 10 m bins from 30 m below the water surface to 300 m water depth, in order to account for surface noise and the near-field range of the 38 kHz echosounder, and the decreased signal-to-noise ratio with depth for the 120 kHz frequency. Acoustic data were not retained for analysis when the vessel speed dropped below 5 knots. We considered NASC a relative index of abundance and a proxy for krill biomass within this depth range.

Nighttime NASC data were filtered out as the diel vertical migration of krill to the surface mixed layer results in the disappearance of part of the krill acoustic signal above the echosounder's range. Although krill can also be found at the surface during the day (Endo, 1984; Smith and Adams, 1988), we considered the daytime NASC to be more representative of krill abundance. The daytime NASC data (one hour after sunrise to one hour before sunset) were therefore summed through the water column and averaged daily over grids of 5 km resolution (Fig. 1a).

2.2.2. Bongo net tow data

Krill were collected at night and dusk at long-term, established

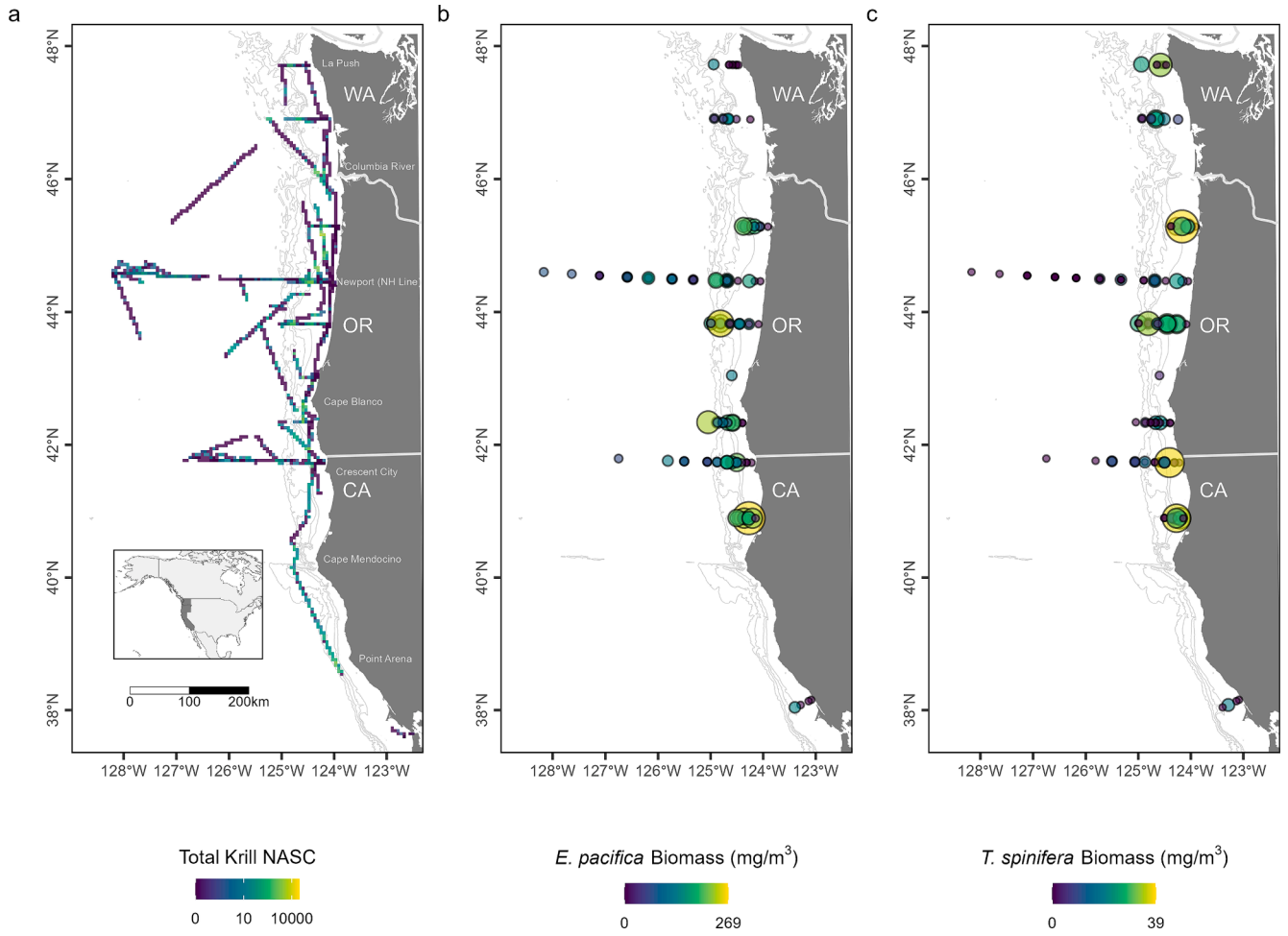

Fig. 1. Maps of study area and a) total krill NASC calculated along transects and aggregated in 5 km resolution grids (daily data are overlayed), b) *E. pacifica* biomass and c) *T. spinifera* biomass estimated from bongo net tows conducted at discrete stations of the NCC surveys along the US West Coast. Maps display data from multiple surveys conducted across five years (2018–2022). Land is shown in dark gray. Isobaths (200 m, 500 m, 1000 m, and 1,500 m deep) are represented with gray lines.

stations (Figure S1, Table S1) by towing a bongo net with a mouth diameter of 0.6 m and 335 μm mesh obliquely through the upper 100 m of the water column. The samples were preserved in 5 % buffered formalin and later processed in the lab where the samples were split using a Folsom splitter. Krill were individually measured and identified to species and developmental stage (juvenile, non-reproductive adult, female, and male). A General Oceanics flowmeter (model 2030) measured the volume of water filtered from each bongo tow, which was used to calculate density (ind. m^{-3}) for each species and life history stage. Density was converted to biomass (mg C. m^{-3}) using dry weight to total length regressions from Fisher et al. 2020 (*E. pacifica*: DW = 0.0008 * TL3.19; *T. spinifera*: DW = 0.004 * TL2.81) and a dry weight to carbon multiplier of 0.45 from (Ross, 1982). More details about the sample processing can be found in Fisher et al. (2020).

A complementary dataset of krill biomass from shallow bongo net tows was used to test and validate the modeled predictions of *E. pacifica* and *T. spinifera* proportions. These data were collected from bongo net tows conducted monthly or bi-monthly year-round since 2001 at five stations along the Newport Hydrographic Line (NH Line, 44.6°N, Figure S1), located 9–46 km from shore (https://www.integratedecosystemassessment.noaa.gov/regions/california-current/newport-hydrographic-line). These oblique bongo tows sampled the upper 25 m of the water column and were conducted at night to target krill that migrated into the surface mixed layer. Because of differences in depth used for sampling methods between the NCC and NH Line, biomass data are not directly comparable. However, we assumed that the relative proportions of *E. pacifica* and *T. spinifera* found in the NH Line tows were representative of the average species proportions in the water column, and therefore appropriate to use as validation for our modeled predictions of each krill species (but not appropriate to be combined with the model training dataset composed of NCC survey samples). The entire NH Line biomass dataset (2001–2022) was used to visually compare model predicted species-scaled NASC to observed biomass averaged by month x year, and then either by month or depth bin. The NH Line biomass dataset collected during this study (2018–2022) was used to numerically validate the predicted proportions of *T. spinifera* and *E. pacifica*.

2.3. Environmental data

Krill distribution was assessed with respect to topographic and dynamic environmental variables known to affect productivity and krill distribution in the central and southern California Current (Cimino et al., 2020; Dorman et al., 2015b; Santora et al., 2018, 2011). Bathymetric charts were obtained from the General Bathymetric Chart of the Oceans (GEBCO, 15 arc-second resolution). Depth (hereafter "DEPTH") and slope (hereafter "SLOPE") were derived from these charts. Depth was log-transformed to increase the contribution of the depth changes on the shallow continental shelf slope compared to the deeper offshore regions. Coastlines were obtained from the OpenStreetMap dataset (https://openstreetmapdata.com/data/coastlines) and used to map data and results. Distance to the closest submarine canyon (CANYON) was calculated from a worldwide geomorphological map (Harris et al., 2014), so that results would be comparable to Santora et al., (2018). Dynamic variables were acquired from daily fields of the near-real time configuration (2011-present) of the Regional Ocean Modeling System (ROMS, Neveu et al., 2016) covering the California Current System from 134°W to the coast, and from 30 to 48°N, with a horizontal resolution of 0.1° (https://oceanmodeling.ucsc.edu:8443/thredds/catalog.html).

Eight variables were derived from ROMS to describe surface and subsurface ocean circulation dynamics: sea surface temperature (SST in °C) and its spatial standard deviation (SSTSD; calculated over 0.3° squares), sea surface height (SSH in m) and its spatial standard deviation (SSHSD; calculated over 0.3° squares), eddy kinetic energy (EKE; calculated from eastward and northward surface current velocities, $kg{\cdot}m^2{\cdot}s^{-2}$), wind stress curl (CURL in $Newton{\cdot}m^{-3}$), isothermal layer depth (ILD in m) and bulk buoyancy frequency (BBV averaged over the upper 200 m, also known as Brunt-Väisälä frequency, in s^{-1}). These variables are good indicators of horizontal and vertical ocean mixing that occur during upwelling events in the spring and summer and have been shown to correlate with the distribution and movements of krill predators (e.g., blue whales, Abrahms et al., 2019; humpback whales, Derville et al., 2022, blue, fin, and humpback whales, Becker et al., 2018). In addition, remotely-sensed daily chlorophyll-a (CHLA) data were acquired from the Aqua MODIS satellite products at 0.025° resolution (ERDDAP: NOAA NMFS SWFSC, https://coastwatch.pfeg.noaa.gov/erddap/info/erdMBchla1day/index.html) to reflect primary productivity in the study system. Daily CHLA layers were averaged over 7 days and interpolated to fill part of the small data gaps from cloud cover with a focal mean calculated over a 0.075° square. ROMS daily layers were slightly extrapolated in the most nearshore waters of the study area where data gaps of 0.1° wide were filled with the average values from the three nearest neighboring cells. EKE and CHLA layers were log10-transformed following (Cimino et al., 2020). All environmental layers were projected in a Universal Transverse Mercator coordinate system to ensure accurate spatial computations within our study area (UTM 10 N) and rescaled to 5-km resolution.

2.4. Modeling framework

2.4.1. Hurdle framework

Krill NASC data were modeled in relation to a series of environmental variables extracted at the center of each daily 5 km x 5 km cell of aggregated acoustic data. Krill biomass data from net samples for each species were similarly modeled using the same environmental variables, matched in space and time to each bongo net tow. For both datasets, and in the case of biomass for both species, the same modeling framework was applied (Figure S2), which consisted of two different statistical algorithms (GAMs and BRTs) and for each of these methods, models were further decomposed with a two-step hurdle approach. With both NASC or biomass data, initial models set all positive values to 1, and the resulting presence / absence data were modeled as a binomial response. Second, all values equal to zero (i.e., absence of krill) were removed, and the resulting abundance conditional on presence was modeled with a Gamma distribution and log link function (GAM) or was log-transformed and modeled with a Gaussian distribution (BRT).

2.4.2. Statistical algorithms

GAMs (Hastie and Tibshirani, 1990) were fitted with the *mgcv* R package (version 1.8–38; Wood, 2011) using a restricted maximum likelihood method. We used penalized thin-plate regression splines for all environmental predictors, with smooth basis size limited to 5 to prevent overfitting. Variable selection was conducted with a shrinkage approach implemented in the *mgcv* R package, which adds an extra penalty to each smoother and penalizes non-significant variables to zero (Marra and Wood, 2011). BRTs (Friedman, 2001) were fitted with the gbm R package (version 2.1.8) with a custom tuning algorithm that iteratively runs the gbm.step function, starting with a learning rate of 0.01 and dividing it by two until the number of trees is above 1000 (Barlow et al., 2020). Models were fitted with an initial number of 50 trees, a tree complexity of 2, and a bag fraction of 0.75.

2.4.3. Environmental predictors

Up to seven different combinations of environmental predictors were tested to identify primary drivers of krill by topographic and dynamic features while avoiding variable collinearity and testing the effect of variable transformations. As collinearity among explanatory variables is known to affect a model's stability, Pearson coefficients were computed beforehand between each pair of variables recorded at the krill NASC data locations and we checked that none exceeded 0.7 (Dormann et al., 2013, Figure S3). The "topographic" model design included only the three topographic variables: DEPTH, SLOPE, and CANYON. The

"dynamic" design included the three topographic variables, plus eight dynamic variables derived from ROMS: SST, SSH, SSTSD, SSHSD, EKE, CURL, BBV, and ILD. The "dynamic-chla" design included all of these eleven variables, plus the satellite-derived CHLA. The "dynamic-log-depth" design was the same as the "dynamic" design except that DEPTH was log-transformed. The "topographic-logdepth" design was similar to the "topographic" design except that DEPTH was log-transformed and was tested only in the biomass model. The "dynamic-sst" design included log-transformed DEPTH, SLOPE, CANYON, and SST and was tested only in the biomass model. The "dynamic-0.6cor" design included a smaller selection of seven variables (DEPTH, SLOPE, SST, SSTSD, SSHSD, ILD, BBV) that passed a stricter collinearity test, by which none of these pairs of variables were correlated with a Pearson coefficient $>$ 0.6. In all dynamic models, dynamic variables were computed at a weekly scale, with daily values averaged over the 7 days prior to any given survey day included in the data. Predictor sets are summarized in Table 1.

2.5. Model evaluation

Models were run with 8-fold (for krill NASC data) and 10-fold (for krill biomass data by species) cross-validation grouped by research cruise to account for the structure of the data. In turn, one of the folds (hence one of the surveys) was withheld for testing and evaluation while the other folds were used to train the model. Since winter conditions were only represented in the NASC data with one survey (February 2020), this survey was not considered as a separate fold to be withheld and rather was always included in the training set. The percentage of deviance explained by each of the model runs was calculated over the training fold. To evaluate the binomial models of presence/absence, the Area Under the ROC Curve (AUC) was calculated both over the training data (AUC.train) and the withheld testing fold (AUC.test). To evaluate the abundance models, the Spearman correlation coefficient and the Pearson correlation coefficient between observed and predicted NASC or biomass were computed in the test fold. Finally, all evaluation metrics were averaged over the 8 or 10-fold model runs.

Functional response plots were produced for each significant environmental predictor across folds (approximate smooth term significance with p-value $<$ 0.05) to visualize the effect of one variable while all others were held constant at their mean. Variable importance was estimated for GAMs as the number of fold runs with significance p-values less than 0.05, 0.01 and 0.001 and for BRTs as the relative influence scaled to 100. This metric reflects the number of times a predictor is selected for splitting and how much it improves the BRT fit (Friedman and Meulman, 2003).

Table 1
Predictor sets tested in the krill NASC and biomass models.

Predictor set name	Topographic predictors	Dynamic predictors
Topographic	DEPTH, SLOPE, CANYON	
Topographic-logdepth	Log-transformed DEPTH, SLOPE, CANYON	
Dynamic	DEPTH, SLOPE, CANYON	SST, SSH, SSTSD, SSHSD, EKE, CURL, BBV, ILD
Dynamic-logdepth	Log-transformed DEPTH, SLOPE, CANYON	SST, SSH, SSTSD, SSHSD, EKE, CURL, BBV, ILD
Dynamic-chla	DEPTH, SLOPE, CANYON	SST, SSH, SSTSD, SSHSD, EKE, CURL, BBV, ILD, CHLA
Dynamic-0.6cor	DEPTH, SLOPE	SST, SSTSD, SSHSD, ILD, BBV
Dynamic-sst	Log-transformed DEPTH, SLOPE, CANYON	SST

Environmental predictors are classified as topographic or dynamic: distance to canyons (CANYON in km), seabed depth (DEPTH in m), seabed slope (SLOPE in radians), sea surface temperature (SST in °C) and its spatial standard deviation (SSTSD calculated over 0.3° squares), sea surface height (SSH in m) and its spatial standard deviation (SSHSD calculated over 0.3° squares), log-transformed eddy kinetic energy (EKE calculated from eastward and northward surface current velocities, $kg{\cdot}m^2{\cdot}s^{-2}$), wind stress curl (CURL in Newton. m^{-3}), isothermal layer depth (ILD in m), bulk buoyancy frequency (BBV in s^{-1}) and satellite-derived chlorophyll-a (CHLA).

2.6. Predicted distributions

2.6.1. Hurdle model predictions

Krill distribution was predicted from 2018 to 2022 at monthly scales on a 5-km resolution grid. For each month, predictions were first computed at a weekly scale, from the last week of the previous month to the third week of the month of interest. Mean predicted krill distribution was calculated across the four weeks, then averaged across the 8 or 10 cross-validation runs. Whether predicting from the total krill NASC models or from the species-specific biomass models, the final predictions were obtained by multiplying the predicted probabilities of presence derived from the presence/absence model (i.e., continuous values $\in$ [0, 1]), with the predicted abundance derived from the abundance model (i.e., continuous values $>$ 0; Phillips et al., 2022). Based on multiple quantitative evaluation metrics described above (AUC.train, AUC.test, Spearman correlation coefficient) and visual assessment of the predictions' ecological credibility, the "optimum" model combination was selected for the total krill NASC models and for the species-specific biomass models. All possible combinations were considered, across the two algorithms (GAM or BRT) and the five predictor sets (topographic, dynamic, dynamic-logdepth, dynamic-chla, dynamic-0.6cor). An "ensemble" combination of models was also considered whereby the results of a presence/absence BRT were combined with that of an abundance GAM.

2.6.2. Species-scaled NASC predictions and evaluation

The final species-specific predictions of *E. pacifica* and *T. spinifera*, termed "species-scaled NASC", were calculated with both the outputs of the krill NASC models and the krill biomass models. First, the monthly predictions derived from the krill biomass models were combined across the two species to calculate the respective proportions of *E. pacifica* and *T. spinifera* predicted to occur at any time and place (e.g., *E. pacifica* proportion = *E. pacifica* predicted biomass / (*E. pacifica* + *T. spinifera* predicted biomass)). At this point, the credibility of the species proportions predictions were also evaluated by comparing them to monthly observed species proportions from the year-round NH Line bongo net tows. This external dataset allowed for an independent evaluation of the seasonal and longitudinal patterns (along the continental shelf to 300 m water depth) predicted by the species-specific krill biomass models. A Pearson correlation coefficient was used to compare observed and predicted proportions along the NH Line and NCC survey stations.

Finally, to derive monthly predictions of species-scaled NASC, the monthly predicted proportions of *E. pacifica* and *T. spinifera*, generated from the optimum species-specific krill biomass model, were multiplied by the monthly NASC predictions of overall krill abundance, generated from the optimum krill NASC model. Predicted species-scaled NASC were then summed by month over the study region to derive a monthly climatological time series of *E. pacifica* and *T. spinifera* abundance from 2018 to 2022 to quantify seasonal differences in the occurrence of the two species. The same time series was also derived only along the latitude of the NH Line to directly compare the temporal and cross-shelf trends of the modeled species-scaled NASC to the observed *E. pacifica* and *T. spinifera* biomass from the NH Line data. To compare trends, predicted and observed values were scaled to 0–100 and linear regressions were conducted to compute slope coefficients.

3. Results

A total of 4,023 km of daytime krill NASC data (equivalent to 1,512 values from 5x5 km average daily grid cells), 118 nighttime and 8 dusk bongo net tows from the NCC surveys, and 112 nighttime bongo net tows

from the NH Line stations were collected and processed across five years (2018–2022, Fig. 1, Figure S4). Krill NASC data ranged from 0 to 29,800 m^2nmi^{-2} with a mean of 102 m^2 nmi^{-2} and median of 0 m^2 nmi^{-2} indicating zero-inflation. *E. pacifica* biomass (mean 10.9 mg C m^3, max 270.0 mg C m^3) captured by the tows at the NCC survey stations was higher than that of *T. spinifera* (mean 2.2 mg C m^3, max 39.4 mg C m^3; Wilcoxon rank sum test: $W = 10905$, $p < 0.001$).

3.1. Krill NASC models

3.1.1. Model selection

As our "optimum" NASC model, we selected the BRT presence/absence model and the GAM abundance model of krill NASC in relation to the dynamic-logdepth predictors to investigate krill habitat use patterns and produce monthly predicted maps of krill NASC. The BRTs performed consistently better than GAMs, with greater deviance explained in the presence/absence NASC model, whereas greater deviance was explained by the GAMs for the abundance model (Table 2). The dynamic-logdepth model displayed the greatest deviance explained across the five predictor sets tested, reaching 24.5 % in the presence/absence BRT model and 48.8 % in the abundance GAM model. When predicting to the training folds, BRTs had consistently higher AUC values than GAMs, whereas when predicting to the test folds, BRTs and GAMs had similar AUC values. This difference between training and test data set performance indicates a potential for slight overfitting by the BRTs compared to GAMs. The dynamic-logdepth models still ranked among the top models under this evaluation metric (BRT dynamic-logdepth AUC.train = 0.948, AUC.test = 0.664). Furthermore, when assessing the performance of the abundance model to predict krill NASC to the test folds, the dynamic-logdepth GAM model also marked the highest scores, measured by a Pearson coefficient of correlation of 0.449 between observed and predicted values. Taken together, these performance metrics supported our choice of an ensemble approach as the best model combination to proceed with.

3.1.2. Predictor influence and trends

In the BRT presence/absence model, the probability of krill NASC presence was predominantly driven by topographic variables: depth (mean influence = 17.2 %) and distance to canyons (mean influence = 12.9 %; Fig. 2a). Indeed, the probability of presence showed a peak at a depth of 250 m (Fig. 2b). Krill probability of presence increased in proximity to canyons between 0 and 100 km, as well as at very large distances (150–250 km). Dynamic predictors had similar contributions around 10 % but showed relatively consistent patterns across folds, which supports the stability of the ecological relationships identified in the functional response plots (Fig. 2b). In the GAM abundance model, krill NASC abundance was driven by depth, sea surface height, wind stress curl, and isothermal layer depth, which were all significant with a 0.001 threshold in at least 7 out of 8 folds (Fig. 2a). Abundance was predicted to increase around a depth of 150 m, as well as when the standard deviation of SST increased, when sea surface height was negative (indicating upwelling favorable and/or equatorward transport), when wind stress curl was negative, and when isothermal layer was more shallow (Fig. 2c).

3.1.3. Predicted maps

The predictions of krill NASC (Fig. 3) resulting from the ensemble predictions of the BRT presence/absence model and the GAM abundance model visualize the ecological relationships identified in Fig. 2. The monthly maps of predictions reflected the expected seasonality (less krill in the winter months) and topographic association (more krill around, and inshore of, the 200 m isobath). The models captured the sharp decline in krill NASC predicted to occur in the most nearshore waters of the inner continental shelf, while offshore waters showed generally low to very low predicted krill NASC (except for discrete offshore patches of relatively high predicted krill NASC in September).

3.2. Krill species-specific biomass models

3.2.1. Model selection

Selecting a single best performing model for each of the two species-specific biomass models was more challenging than selecting the best NASC model, as performance metrics showed contrasting results, and models were generally more unstable due to smaller sample sizes. Across both krill species, GAMs generally performed better in terms of deviance explained, while BRT had greater AUC values when calculated over the training folds (AUC.int, Table 3). Considering the relatively small sample size applied in this cross-validation (n = 126 station samples) and

Table 2
Performance metrics of the krill NASC model.

Model type	Predictors	Method	Dev (%)	AUC.train	AUC.test	Pearson	Spearman
presence/absence model	dynamic-logdepth	BRT*	24.512	0.948	0.664		
	dynamic-chla	BRT	24.45	0.954	0.644		
	dynamic	BRT	23.7	0.947	0.657		
	dynamic-0.6cor	BRT	21.625	0.929	0.649		
	dynamic-logdepth	GAM	18.387	0.78	0.679		
	dynamic-chla	GAM	17.325	0.772	0.642		
	dynamic	GAM	14.912	0.753	0.662		
	topographic	BRT	13.012	0.799	0.684		
	dynamic-0.6cor	GAM	10.113	0.71	0.655		
	topographic	GAM	7.95	0.693	0.662		
Abundance model	dynamic-logdepth	GAM*	48.788			0.449	0.34
	dynamic-chla	GAM	44.362			0.166	0.206
	dynamic	GAM	41.825			0.168	0.216
	dynamic-0.6cor	GAM	37.138			0.23	0.18
	dynamic-chla	BRT	30.562			0.355	0.318
	dynamic	BRT	29.625			0.343	0.31
	dynamic-logdepth	BRT	29.562			0.349	0.314
	dynamic-0.6cor	BRT	27.925			0.343	0.306
	topographic	GAM	26.025			0.34	0.183
	topographic	BRT	21.363			0.405	0.344

All metrics are averaged over the 8 folds of the cross-validation. Abbreviations: dev (%) = deviance explained by the model; AUC.train = Area Under the roc Curve calculated over the training folds; AUC.test = Area Under the roc Curve calculated over the test folds; Pearson = Pearson correlation coefficient calculated over the test folds; Spearman = Spearman rank correlation coefficient calculated over the test folds. Models are ranked by deviance explained and asterisks indicate the models selected for the ensemble approach.

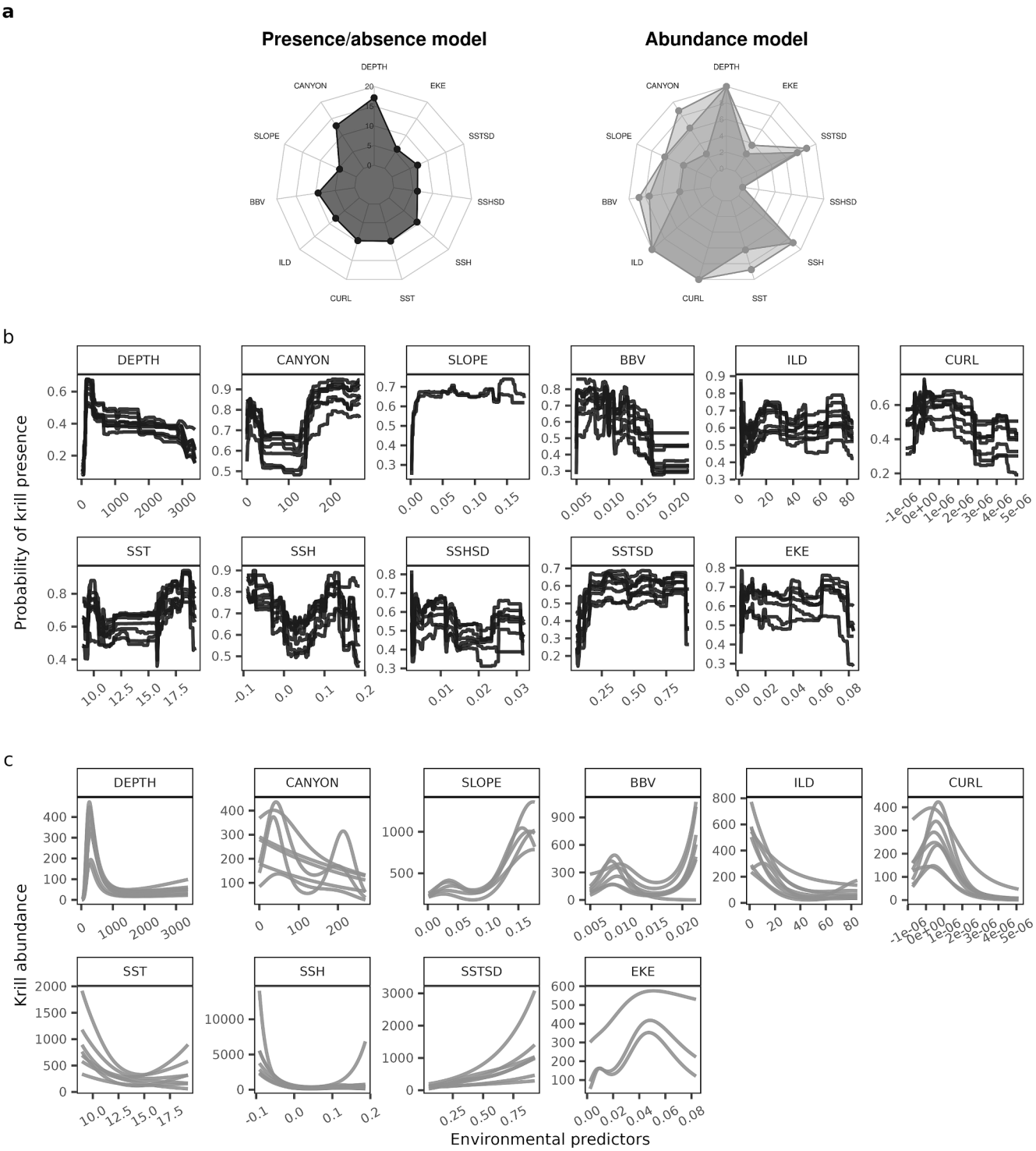

Fig. 2. Predictor contributions (a) and partial response plots representing the probability of krill presence (b) and krill abundance (c) as predicted by the hurdle models of total krill NASC (BRT and GAM respectively for b and c). Functional response curves represent the effect of a predictor upon the trend in krill probability of presence or abundance. Solid lines represent the marginal effect of each variable relative to krill per cross-validation fold. Only the variables with a contribution of more than 5 % (BRT) or an approximate smooth significance p-value < 0.05 (GAM) are shown per model fold. Predictor contributions to each of these models are illustrated as radar plots and measured either by the percent of contribution estimated in the BRT presence/absence model or by the number of cross-validation folds in which the approximate smooth significance p-values were below 0.05, 0.01 or 0.001 (shown with increasingly dark color shades) in the GAM abundance model. Environmental predictors are the following: distance to canyons (CANYON in km), log-transformed seabed depth (DEPTH in m), seabed slope (SLOPE in radians), sea surface temperature (SST in °C) and its spatial standard deviation (SSTSD calculated over 0.3° squares), sea surface height (SSH in m) and its spatial standard deviation (SSHSD calculated over 0.3° squares), log-transformed eddy kinetic energy (EKE calculated from eastward and northward surface current velocities, $kg{\cdot}m^2{\cdot}s^{-2}$), wind stress curl (CURL in $Newton.m^{-3}$), isothermal layer depth (ILD in m) and bulk buoyancy frequency (BBV in s^{-1}).

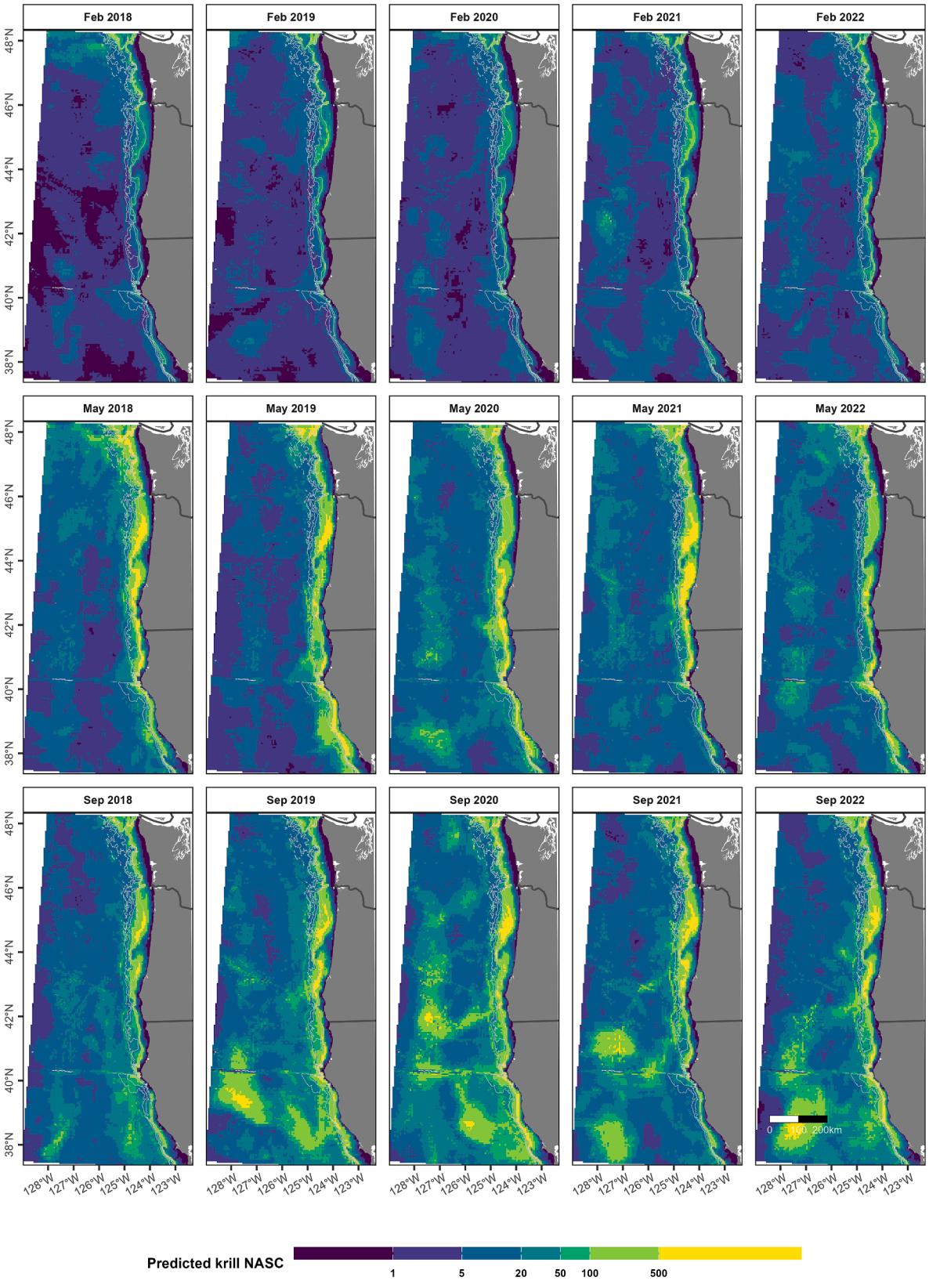

Fig. 3. Monthly maps of predicted krill NASC for the months of February, May, and September 2018–2022. Maps are obtained by multiplying weekly predictions from the krill presence/absence model and the krill abundance model and averaging the outputs by month. Abundance is shown on a log-transformed color scale, with purple indicating lower values and yellow indicating higher values. Land is shown in dark gray. Isobaths (200 m, 500 m, 1000 m, and 1,500 m deep) are represented with gray lines. Latitude and longitude coordinates of the maps are shown on the left and bottom panels respectively. (For interpretation of the references to color in this figure legend, the reader is referred to the web version of this article.)

Table 3
Performance metrics of the krill species-specific biomass models. All metrics are averaged over the 10 folds of the cross-validation.

Species	Model type	Predictors	Method	Dev (%)	AUC.train	AUC.test	Pearson	Spearman
E. pacifica	Presence/absence model	dynamic-chla	GAM	93.3	0.998	0.863		
		dynamic	GAM	93.06	0.998	0.932		
		dynamic-logdepth	GAM	90.17	0.996	0.863		
		dynamic-0.6cor	GAM	70.44	0.979	0.929		
		dynamic-sst	GAM	58.62	0.962	0.935		
		topographic-logdepth	GAM	58.21	0.963	0.938		
		topographic	BRT	57.8	0.991	0.895		
		dynamic-0.6cor	BRT	57.71	0.995	0.904		
		topographic-logdepth*	BRT	57.53	0.991	0.895		
		topographic	GAM	56.86	0.963	0.938		
		dynamic-chla	BRT	56.79	0.995	0.901		
		dynamic	BRT	56.5	0.996	0.901		
		dynamic-logdepth	BRT	56.21	0.996	0.901		
		dynamic-sst	BRT	55.74	0.993	0.904		
	Biomass model	dynamic-chla	GAM	37.88			0.388	0.396
		dynamic-logdepth	GAM	35.57			0.237	0.347
		dynamic	GAM	35.28			0.234	0.348
		dynamic-0.6cor	GAM	29.03			0.325	0.42
		topographic	GAM	23.43			0.27	0.411
		dynamic-sst	GAM	22.26			0.246	0.408
		topographic-logdepth*	GAM	22.26			0.246	0.408
		topographic-logdepth	BRT	15.12			0.456	0.377
		topographic	BRT	13.52			0.454	0.372
		dynamic-0.6cor	BRT	13.1			0.398	0.391
		dynamic-sst	BRT	12.52			0.443	0.383
		dynamic-logdep	BRT	9.09			0.402	0.406
		dynamic	BRT	8.74			0.427	0.362
		dynamic-chla	BRT	8.67			0.437	0.446
T. spinifera	Presence/absence model	dynamic-sst	GAM	20.38	0.753	0.704		
		topographic-logdepth	GAM	20.38	0.752	0.704		
		dynamic-logdepth	GAM	18.03	0.772	0.62		
		dynamic	GAM	15.83	0.751	0.63		
		dynamic-chla	GAM	14.92	0.742	0.609		
		topographic	BRT	13.76	0.888	0.712		
		topographic-logdepth*	BRT	13.31	0.891	0.738		
		topographic	GAM	11.95	0.608	0.635		
		dynamic-sst	BRT	10.81	0.908	0.727		
		dynamic-0.6cor	GAM	8.52	0.691	0.583		
		dynamic-0.6cor	BRT	4.92	0.895	0.662		
		dynamic	BRT	4.62	0.901	0.647		
		dynamic-chla	BRT	4.46	0.903	0.642		
		dynamic-logdepth	BRT	3.55	0.897	0.64		
	Biomass model	dynamic-chla	GAM	51.8			0.565	0.479
		dynamic-logdepth	GAM	50.34			0.5	0.453
		dynamic	GAM	40.51			0.522	0.53
		dynamic-sst	GAM	35.78			0.494	0.383
		dynamic-0.6cor	GAM	34.14			0.483	0.521
		dynamic-0.6cor	BRT	28.42			0.392	0.334
		topographic-logdepth*	GAM	27.01			0.403	0.416
		topographic	BRT	21.75			0.504	0.559
		topographic	GAM	21.69			0.474	0.436
		dynamic	BRT	21.23			0.432	0.459
		dynamic-sst	BRT	20.94			0.438	0.419
		dynamic-logdepth	BRT	18.62			0.415	0.472
		topographic-logdepth	BRT	15.75			0.496	0.498
		dynamic-chla	BRT	11.72			0.424	0.37

Abbreviations: dev (%) = deviance explained by the model; AUC.train = Area Under the roc Curve calculated over the training folds; AUC.test = Area Under the roc Curve calculated over the test folds; Pearson = Pearson correlation coefficient calculated over the test folds; Spearman = Spearman rank correlation coefficient calculated over the test folds. Models are ranked by deviance explained and asterisks indicate the models selected for the ensemble approach.

therefore the small number of stations that could be withheld in each test fold (from 3 to 21), we chose not to rely on the test fold performance metrics (AUC.ext, Pearson and Spearman coefficients) to select the optimum predictor set for the next steps of the analysis. Training fold performance metrics were favored instead. While the GAMs applied with the dynamic-chla or dynamic-logdepth predictors performed well in terms of deviance explained (Table 3), further visual inspection of the predictions revealed extrapolation issues, where unrealistically high krill biomass was predicted in the winter and/or offshore for *T. spinifera* (Figure S5). Predictor contribution percents showed that these dynamic models were mostly driven by topographic variables, indicating that the simpler topographic predictor set may be more appropriate and conservative (Figure S6). Similarly, the dynamic-sst model that only included the three topographic predictors and SST, showed unrealistic predictions and was rejected.

To help select the optimum presence/absence and biomass model, the predicted proportions of *E. pacifica* and *T. spinifera* biomass from the six most well-performing combinations of models were computed at the time and location of each NCC (n = 126) and NH Line (n = 112) sampling station to compare the model-derived species proportions to the

observed proportions. We found a correlation of $r^2 = 0.59$ ($p < 0.001$) between observed and predicted proportions from the ensemble BRT / GAM biomass models applied to the topographic-logdepth design, which was higher than those obtained from our other top model candidates (Figure S7). This comparison validated the ensemble approach with topographic-logdepth predictors as the optimum modeling approach for *E. pacifica* and *T. spinifera* biomass.

3.2.2. Predictor influence and trends

In the ensemble model of *E. pacifica* and *T. spinifera* biomass, bottom depth dominated the presence/absence models for both species, but particularly in the *E. pacifica* model where it contributed greater than 90 % of the variance (Fig. 4a). Higher probability of presence was predicted in depths of 100 m and deeper for *E. pacifica*, and shallower than 200 m for *T. spinifera* (Fig. 4b), with a particularly strong agreement between cross-validation folds in the *E. pacifica* depth fitted relationships. *T. spinifera* presence was also strongly influenced by proximity to canyons (Fig. 4b). Conditional on presence, steep slopes correlated with higher *E. pacifica* biomass (Fig. 4c), a pattern that is to be expected along the shelf break. Both species were predicted to increase in biomass in depths shallower than 200 m.

3.2.3. Predicted maps

The marked patterns of species-specific distribution with respect to seabed topography were reflected in the predicted maps of *E. pacifica* and *T. spinifera* proportion (%), representing the probability of encountering one species over the other (Fig. 5 and Figure S6 for cropped or full extent maps respectively). Overall, *E. pacifica* dominated the proportions (median predicted proportions across study area 95 % *E. pacifica*, 5 % *T. spinifera*), particularly just offshore of the shelf break, and on the slope and off-shelf habitats, while *T. spinifera* were most prevalent on the shelf in waters < 200 m of depth. There were regions where both species overlapped. These regions were mainly concentrated along, and just inshore of, the 200 m isobath.

3.3. Species-scaled NASC predictions

3.3.1. Predicted maps

Finally, predicted proportions of *E. pacifica* and *T. spinifera* combined with predicted krill NASC allowed us to derive weekly and monthly predictions of species-scaled NASC across the NCC region. Predictions averaged by month showed a clear difference in habitat preference between *T. spinifera* that is constrained to the shelf, around and inshore of the 200 m isobath, and *E. pacifica* that is found in high abundance just

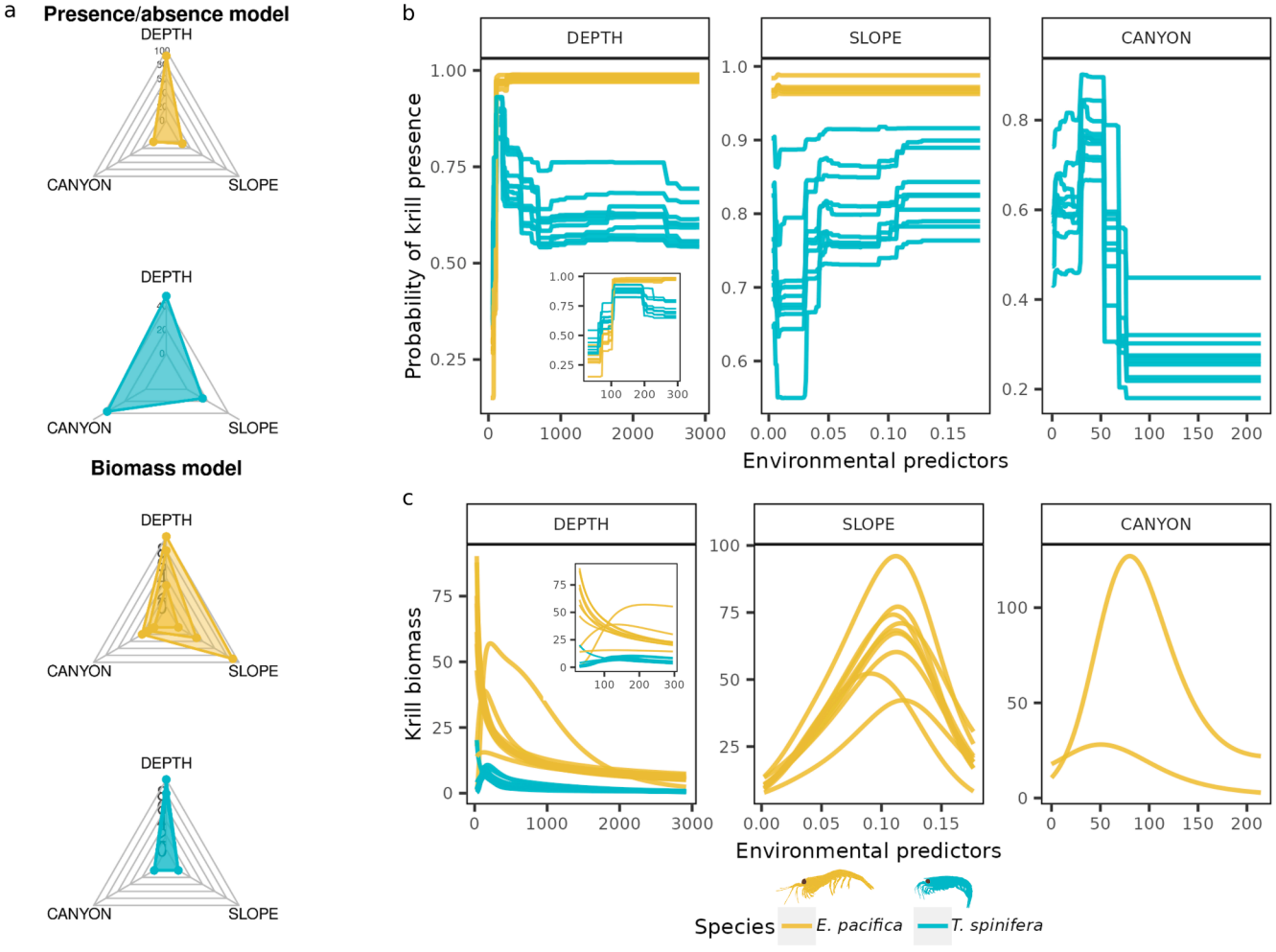

Fig. 4. Predictor contributions to species-specific models of krill biomass (a) and functional response curves representing the effect of the main predictors on the trend in krill probability of presence (BRT; b) or biomass (GAM; c). Solid lines represent the marginal effect of each variable relative to krill per cross-validation fold. Only the variables with a contribution of more than 5 % (BRT) or an approximate smooth significance p-value < 0.05 (GAM) are shown per model fold. Predictor contributions are measured either by the percent of contribution estimated in the BRT presence/absence model or by the number of cross-validation folds in which the approximate smooth significance p-values were below 0.05, 0.01 or 0.001 (shown with increasingly dark color shades) in the GAM abundance model. Environmental predictors shown on the x-axis (b, c) are the following: distance to canyons (CANYON in km), log-transformed seabed depth (DEPTH in m), and seabed slope (SLOPE in radians). An inset graph shows the relationship to DEPTH in the inner 300 m.

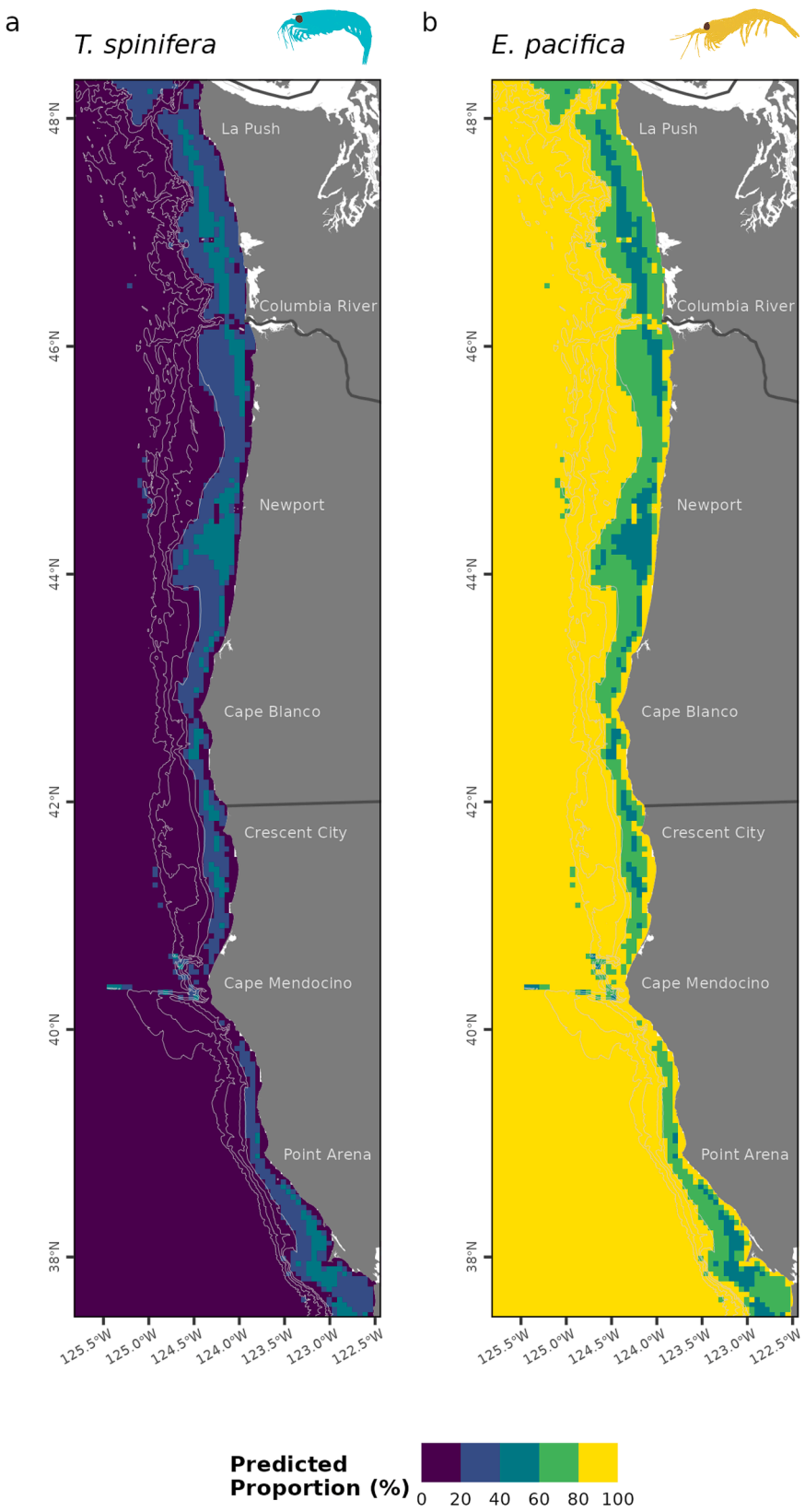

Fig. 5. Predicted proportion of *Euphausia pacifica* and *Thysanoessa spinifera* biomass on the continental shelf and slope (full predictions extent available in Figure S8). Note that predictions of proportions are only based on topographic variables and are therefore static through time. Land is shown in dark gray. Isobaths (200 m, 500 m, 1000 m, and 1,500 m deep) are represented with gray lines.

offshore of the 200 m isobath and further offshore in lower abundance (Figs. 6 and 7). The latitudinal distribution of *T. spinifera* was also predicted to be more skewed to the north of the study area where the shelf is wider. This cross-shelf species-specific pattern matched the biomass observed at stations along the NH Line off Newport over the long term (2001–2022) and over recent years (2018–2022; Fig. 8). *E. pacifica* increased as a function of log-transformed depth at a similar rate in the predicted NASC values (linear regression coefficient estimate = 69.3 ± SE 7.0; Fig. 8b) and NH Line observed biomass values (linear regression coefficient estimate = 78.3 ± SE 9.3; Fig. 8c).

3.3.2. Seasonal and annual variability

The climatology of monthly species-scaled NASC showed that *E. pacifica* was more abundant during each month than *T. spinifera*, and both species displayed a strong seasonal trend (Fig. 7). The species-scaled NASC of both species increased in the spring and summer, followed by a rapid decline in abundance in the fall (Sep-Nov), and the lowest abundance occurred during the winter months. Both *E. pacifica* and *T. spinifera* species-scaled NASC were predicted to decrease slightly during the month of June. While the species-scaled NASC of both species was highest in August, the variability in predicted patterns across years was also the highest during this month, indicating interannual or spatial variation in peak abundance. Note that since the selected species-specific biomass models only included topographic variables, the inter-annual and seasonal variability in the final species-scaled NASC predictions originates from the NASC models and is the same across species in Fig. 7. These seasonal patterns, including the drop in abundance in June, follow those found in the monthly year-round observational sampling along the NH Line (Figure S9). *E. pacifica* increased between February and August, then decreased between August and December at similar rates in the predicted NASC values (linear regression coefficient estimates = Feb-Aug 14.5 ± SE 1.8, Aug-Dec −21.7 ± SE 4.0; Figure S9a) and NH Line observed biomass values (linear regression coefficient estimates = 7.8 ± SE 3.7, Aug-Dec –22.3 ± SE 4.3; Figure S9b). Similarly, *T. spinifera* increased between February and August, then decreased between August and December at similar rates in the predicted NASC values (linear regression coefficient estimates = 15.7 ± SE 2.3, Aug-Dec −21.8 ± SE 4.1; Figure S9a) and NH Line observed biomass values (linear regression coefficient estimates = 15.6 ± SE 4.7, Aug-Dec −21.2 ± SE 7.7; Figure S9b). Inter-annual variability is illustrated in the monthly predictions for August for each year of the study (Fig. 9). The areas of highest variability are also those with the highest predicted NASC, illustrating the strong fluctuations of resource availability that are faced by predators. Areas of stronger inter-annual variability include the shelf waters north of Cape Mendocino, off Cape Blanco, and south of Heceta Bank.

4. Discussion

This study expands on prior krill modeling efforts in the California Current region by producing fine-scale (5 km resolution) and year-round predictions of *E. pacifica* and *T. spinifera* krill distribution with models that were trained to fit environmental relationships specific to the NCC region. Our study also provides a new methodology for scaling continuous hydroacoustics backscatter to species-specific krill abundance estimates using long-term data from plankton net sampling. With this analytical advancement, our models describe the contrasting abundance and distribution patterns of these two critically important prey species in the NCC. Furthermore, the models can derive species-specific, high resolution spatial predictions of krill abundance that can be incorporated into multiple marine predator studies in the NCC to inform management efforts.

Previous modeling efforts using hydroacoustics to estimate krill abundance do not distinguish the backscatter signal between the two dominant krill species in the California Current (Phillips et al., 2022; Rockwood et al., 2020; Santora et al., 2012) because the size range of these two species overlaps (Siegel, 2000) as well as their expected target strengths and frequency responses (Phillips et al., 2022). Thus, direct sampling of target species is required to apportion the backscatter. Concurrent trawl sampling has been used in previous research to scale acoustic backscatter to estimates of generalized krill biomass (Rockwood et al., 2020), or to infer target species through correlations of backscatter to species biomass estimates (Santora et al., 2011). Average cross-shelf distribution of *E. pacifica* and *T. spinifera* from net samples was also used to estimate the proportion of the backscatter attributable to each species (Dorman et al., 2023). While continuous hydroacoustic datasets provide opportunities to estimate krill abundance over large spatial areas, without species-specific biomass estimates, research on species-specific habitat preferences and spatiotemporal distributions is limited, and can only be inferred from previous research on cross-shore and latitudinal differences between the two species. Employing the methods presented in this study to scale continuous underway hydroacoustic data to apportion *E. pacifica* and *T. spinifera* abundances using estimates from net sampling greatly improves our understanding of the spatiotemporal distribution of these two important forage species. Moreover, our integrative approach to derive species-scaled NASC can be applied to other regions and ecosystems where acoustically detectable species cannot be discriminated based on backscatter alone.

The modeled habitat associations of *E. pacifica* and *T. spinifera* were consistent with prior work in the California Current that demonstrated the influence of the continental shelf break as a feature of where krill accumulate, and to the cross-shelf pattern of species-specific habitat selection (Cimino et al., 2020; Dorman et al., 2015b; Rockwood et al., 2020; Santora et al., 2011). In the final predictions (Figs. 6 and 8), the 200 m isobath is an important boundary between preferential *T. spinifera* habitat (on the shelf) and *E. pacifica's* more cosmopolitan habitat (over the shelf break and offshore). Proximity to canyons was also confirmed as an influential variable for *T. spinifera* but not for *E. pacifica.* Canyons have been shown to aggregate krill in the California Current (Santora et al., 2018), but our species-specific methods suggest that this response might differ by species. Overall, predictions align with the known dominance of *E. pacifica* over *T. spinifera* across the region. *E. pacifica* densities are often referred to as being one order of magnitude greater than *T. spinifera* in the NCC (as per Shaw, unpublished data, referenced in Feinberg et al., 2013; Rockwood et al., 2020) and long-term biomass records along the NH Line show a similar ratio of about 10:1 (Peterson et al., 2017). In our predictions, the ratios of species-scaled NASC were very similar, with an average ratio of 10:1.3, which adds confidence in the quality of our krill distribution models.

In addition to *E. pacifica* and *T. spinifera* being strongly associated with topographic features, the monthly predictions also showed strong seasonal and interannual patterns of abundance, which could have implications for migrating predators. Both species were most abundant during the spring and summer upwelling months, with the highest abundance occurring in August. However, predicted abundances were also the most variable during this period, indicating both interannual and spatial variability in this important prey resource. Indeed, during August, when krill abundance was highest, spatially explicit aggregations occurred, but their location and intensity varied throughout the five years of this study (Fig. 9). These aggregations occurred just north of known upwelling centers, north of Cape Blanco and Cape Mendocino, and in regions with shallow banks and retentive circulation features along the Stonewall and Heceta Bank region (Checkley and Barth, 2009). Similar spatial dissociation between krill aggregations and upwelling centers were found off Central California (Santora et al., 2011) and krill concentration in retentive recirculating features was observed to the north of our study region (Phillips et al., 2022). Interannual changes in the intensity and location of these aggregations is likely due to variation in oceanographic forcing, which has been identified as drivers in other regions of the California Current (Fiechter et al., 2020). Although the geographic extent and magnitude of these aggregations

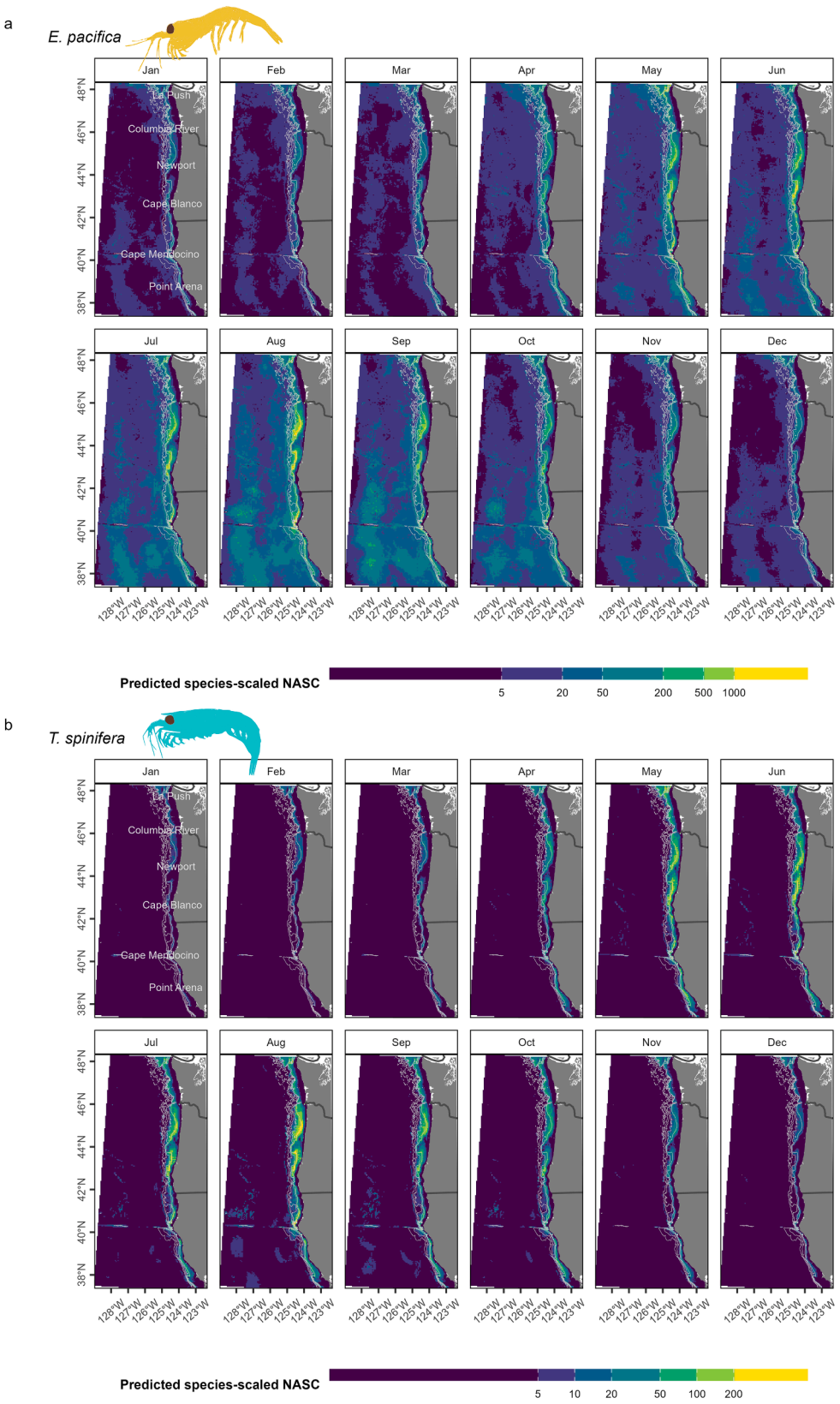

Fig. 6. Monthly average maps of predicted krill species-scaled NASC, a) *Euphausia pacifica*, and b) *Thysanoessa spinifera*. Average monthly predictions are calculated across five years, 2018–2022. Maps are obtained by multiplying predictions of krill NASC and predictions of species proportions. Species-scaled NASC is shown on a log-transformed color scale, with purple indicating lower values and yellow indicating higher values. Land is shown in dark gray. Isobaths (200 m, 500 m, 1000 m, and 1,500 m deep) are represented with gray lines. Latitude and longitude coordinates of the maps are shown on the left and bottom panels respectively. (For interpretation of the references to color in this figure legend, the reader is referred to the web version of this article.)

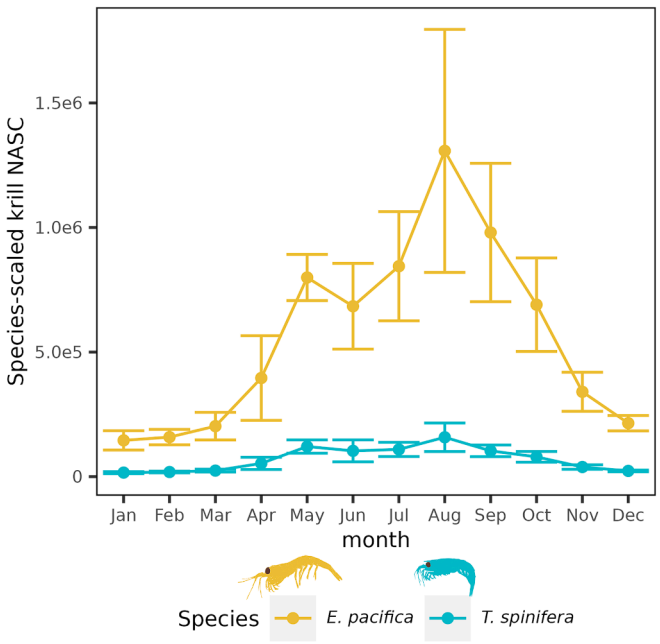

Fig. 7. Predicted krill species-scaled NASC, for *Euphausia pacifica* and *Thysanoessa spinifera* per month, averaged across five years (2018–2022). Error bars represent the standard deviation around the mean abundance that was calculated as the sum of predicted grid cells values across the study area.

changed interannually, the retentive region of Stonewall and Heceta Bank had the highest and the most consistent abundance for both *E. pacifica* and *T. spinifera*. This finding was similar to that of Phillips et al., (2022), who found the most consistent biomass in the recirculation feature of the Juan de Fuca eddy to the north. These two recirculation features in the NCC are known to concentrate phytoplankton that krill feed on (Hickey and Banas, 2008), and they may be persistent features where predators can predictably find prey (Bliss et al., 2024).

Like any other model, our krill distribution models provide a useful yet imperfect representation of reality. Our framework (Figure S2) involved a series of methodological choices informed by a combination of quantitative performance metrics and qualitative considerations, following best practices of marine species distribution modeling (Derville et al., 2018; Elith and Leathwick, 2009; Qiao et al., 2015; Roberts et al., 2017; Robinson et al., 2011). First, even if our two statistical approaches (penalized GAM and BRT) were inherently capable of selecting the predictors that most contributed to explaining the variance observed in krill NASC and biomass, we still assessed the added value of each predictor. For instance, while chlorophyll-a has been used as a predictor of ocean productivity and krill abundance (Cimino et al., 2020; Phillips et al., 2022) and seemed to contribute to our models (Table 2) it was not favored in our optimum models due to data gaps from cloud cover and the loss in operability that would necessitate integrating a satellite-derived data product into our framework. Second, multiple performance metrics, as well as expected predictive outcomes, were considered to select optimum models at each of the framework steps (NASC model, *E. pacifica* biomass model, *T. spinifera* biomass model). For instance, while the deviance or AUC metrics pointed to differences between the models of the two species, we selected the same ensemble approach for *E. pacifica* and *T. spinifera* biomass to ensure comparability of predictions. Finally, visual examination of predictions and comparison to observed biomass values from the NH Line was important to select optimum models, regardless of the performance metrics. Thus, despite higher deviance explained, our dynamic species-specific biomass models suffered from outer-shelf unrealistic predictions (likely due to less data being available offshore) and had to be discarded in favor of more parsimonious topographic models. While this static modelling of biomass limits the capacity to assess how *E. pacifica* and *T. spinifera* may differentially respond to environmental change, it was the most realistic and conservative description of biomass observed in NCC survey net tows. Future extensions of our modeling framework, incorporating additional net tow biomass data, should focus on integrating dynamic predictors into this part of the model, as the temporal variability in the distributions of *E. pacifica* and *T. spinifera* likely impacts the spatial behavior of mobile predators.

Model transferability (i.e. predictions under novel environmental conditions) remains a challenge in species distribution models (Bouchet et al., 2019; Yates et al., 2018) and must be considered in future applications of our krill predictions. Non-stationarity of krill ecological relationships in space and time may limit the robustness of our predictions in the future or in other parts of the California Current region. Our models trained using five years of data did not cover all potential environmental conditions that may occur in the NCC and the robustness of predictions during future extreme climatic events such as marine heatwaves may be challenged (Muhling et al., 2020). Model transferability in space warrants caution as spatial sampling bias may cause environmental variables to be unevenly or incompletely sampled. This bias can increase uncertainty of trends fitted in undersampled environmental space. For instance, the bimodal trend fitted between krill NASC and distance to canyons was likely influenced by uneven sampling with respect to these fixed topographic features. The increased NASC predicted in regions distant to canyons (>150 km) could be the result of other confounding factors and should be considered with caution as it is likely not transferable to other geographic areas. Moreover, predictions in the winter months and waters south of the Oregon-California border should be considered with caution as these period and region were subject to less sampling effort (Table S1, Figure S4). Predictions of species-habitat relationships may also be non-stationary across geographical domains. For instance, simulated distributions of krill hotspots in central-northern California showed high geographical variability in terms of how they associated with centers of upwelling (Dorman et al., 2015b). Similarly, rorqual whale models trained with data collected in the NCC showed different relationships than those trained with central and southern California Current data (Derville et al., 2022). Therefore, comparing the predictions respectively generated by models trained using NCC (the present study) and Central-Southern California (Cimino et al., 2020; Rockwood et al., 2020) data would provide an unprecedented and informative understanding of prey-predator adaptations to local marine processes.

Krill are important prey to many ecologically and commercially important species including marine mammals listed in the Endangered Species Act. *E. pacifica* biomass are ten fold higher than that of *T. spinifera*, while *T. spinifera* are the more energetically profitable species (Fisher et al., 2020). These important differences in prey energetics and abundance likely influence predator selection of prey resources (Nickels et al., 2018). Thus, providing species-specific predictions of their abundance and distribution will provide the explanatory layers needed to develop a better understanding of predator distributions and foraging energetic needs. In this study, both species of krill had the highest abundances during spring and summer, coincident with their highest total lipid content (Fisher et al., 2020). Although the lipid content in both species is higher during the upwelling season, *T. spinifera* have over four times the total lipids per body weight, and they are larger in size compared to *E. pacifica*. The spatial segregation of the two species implies strong cross-shelf differences in lipid content available to predators, with higher concentration of lipid-rich *T. spinifera* on the continental shelf and the more abundant, but less lipid dense *E. pacifica* concentrated along and offshore of the shelf break. Changing ocean conditions could disrupt the distribution and abundance of lower trophic level prey to energy dependent large marine predators. The nearshore affinity for *T. spinifera* likely reflects their association with cooler ocean temperatures and a diatom-rich food source (Fisher et al., 2020). During the 2014–2016 NE Pacific marine heatwave, the density and

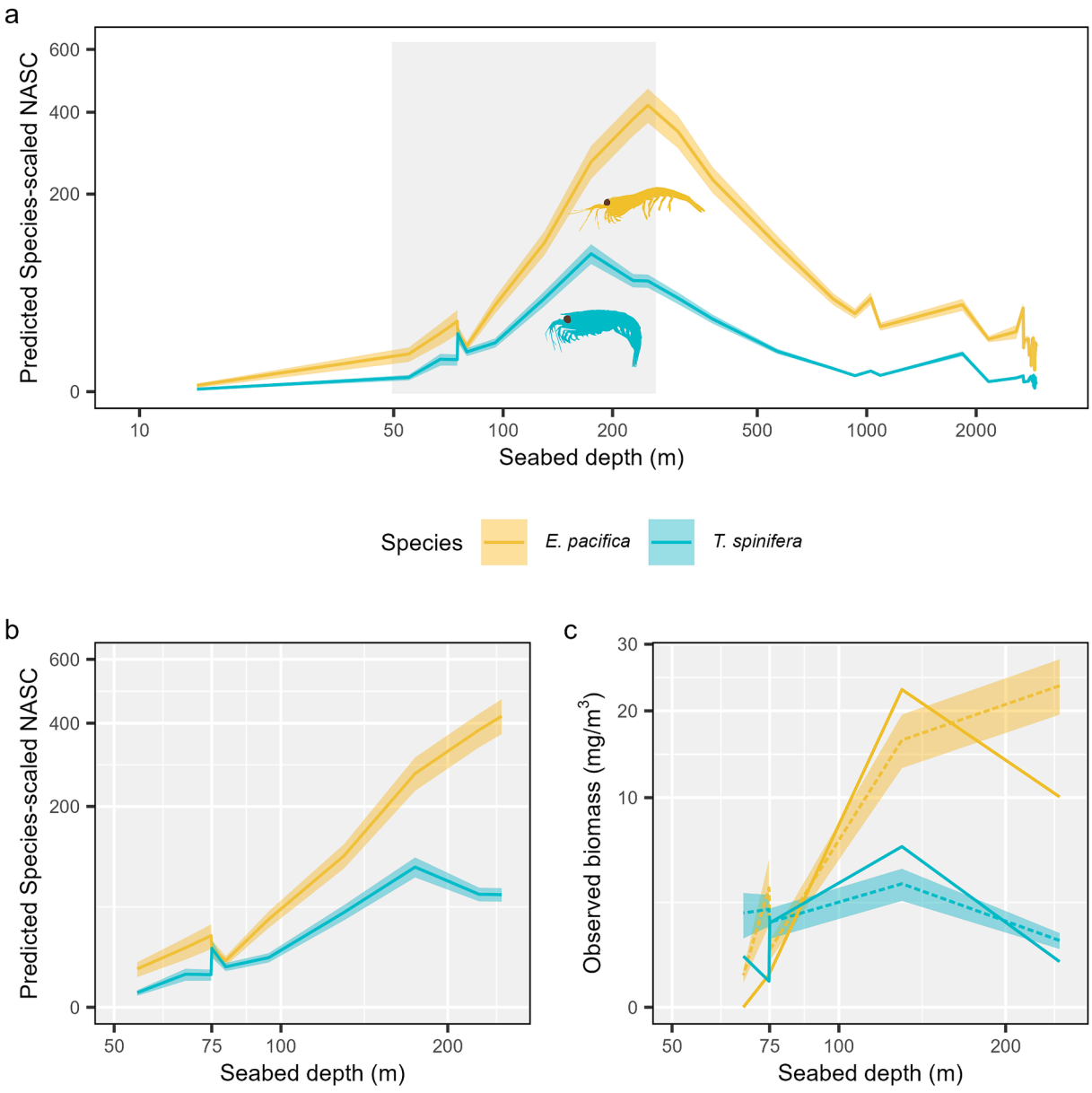

Fig. 8. Predicted (a, b) vs observed (c) patterns of krill species-scaled NASC and biomass at the latitude of the NH Line in relation to seabed depth. Panel a shows the summed predicted species-scaled NASC for each species averaged by year and month, and then by depth. The bottom panel b shows the same predicted trend within the depth range 50 to 250 m covered by the NH Line stations NH05, NH10, NH15, NH20, and NH25. Panel c shows the mean observed biomass per species in 2001–2022 (dotted line and ribbon) and 2018–2022 (solid line) averaged by year and month, and then by depth bin. The x-axis is log transformed and the y-axis is square-root transformed for optimal visualization with the least deformation. Colored ribbons represent the standard error of the average across month x year by depth bin.

biomass of *E. pacifica* decreased dramatically and they were smaller in size, while *T. spinifera* were almost completely absent (Peterson et al., 2017; Robertson and Bjorkstedt, 2020). A warming global ocean compounded with the prediction that marine heatwaves will become more frequent and intense, could have serious impacts on pelagic predators in search of patchy and dynamic prey (Frölicher and Laufkötter, 2018; Oliver et al., 2019).

Krill are an essential component of the NCC ecosystem. Thus, this study provides the foundation for future ecosystem hypotheses testing across the NCC food web and for managing current and emerging threats. Collated with predator distribution data, the predictions of *E. pacifica* and *T. spinifera* will allow researchers to investigate the foraging behavior of predators and clarify the behavioral choices by which they balance their energetic needs in a highly dynamic environment. Such fine scale, widely extensive, and dynamic predictions of krill will provide key information to describe how environmental fluctuations and prey availability have shaped the phenology and life history of predators foraging in the NCC. In a context of rapid climate change and a growing human footprint in the oceans, our predictive distribution models will help assess the times and places where krill-eating predators are most at risk of interacting with human activities such as ship traffic, fishing, and offshore energy development.

CRediT authorship contribution statement

S. Derville: Writing – original draft, Methodology, Funding acquisition, Formal analysis, Conceptualization. **J.L. Fisher:** Writing – original draft, Methodology, Funding acquisition, Data curation, Conceptualization. **R.L. Kaplan:** Writing – review & editing, Formal analysis, Data curation. **K.S. Bernard:** Writing – review & editing,

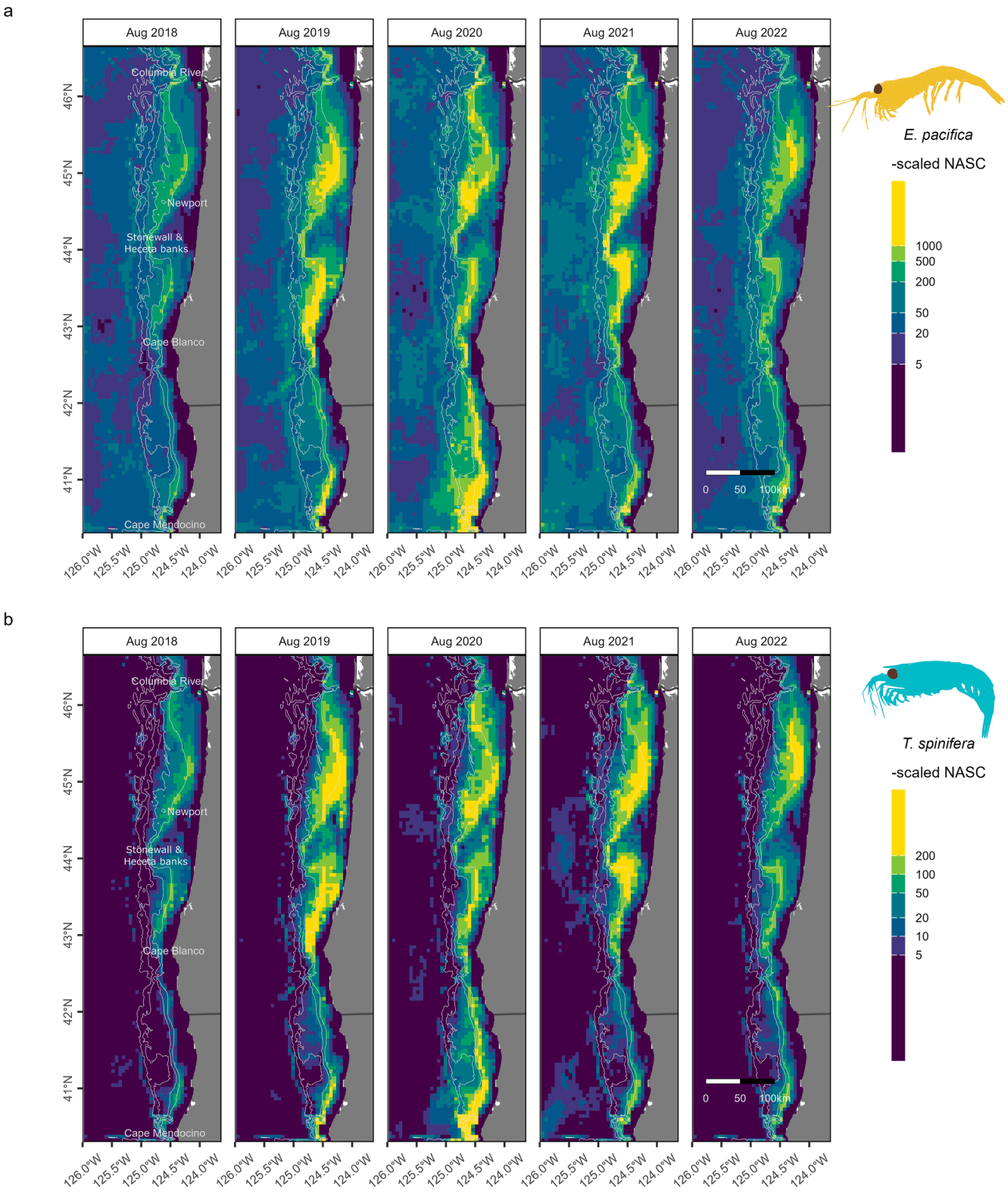

Fig. 9. Monthly maps of predicted krill species-scaled NASC, for a) *Euphausia pacifica*, and b) *Thysanoessa spinifera* for the month of August from 2018 to 2022. Species-scaled NASC is shown on a log-transformed color scale, with purple indicating lower values and yellow indicating higher values. Land is shown in dark gray. Isobaths (200 m, 500 m, 1000 m, and 1,500 m deep) are represented with gray lines. (For interpretation of the references to color in this figure legend, the reader is referred to the web version of this article.)

Funding acquisition, Conceptualization. **E.M. Phillips:** Writing – review & editing, Methodology. **L.G. Torres:** Writing – review & editing, Supervision, Methodology, Funding acquisition, Formal analysis, Conceptualization.

Declaration of competing interest

The authors declare that they have no known competing financial interests or personal relationships that could have appeared to influence

the work reported in this paper.

Acknowledgments

Financial support was provided by the NOAA Species Recovery Grant (#NA22NMF4720105). We would like to acknowledge NOAA Fisheries for ship time and the Bell M Shimada Captain and crew for sampling support. We would like to acknowledge Tracy Shaw, Ashley Hudson, Amanda Kent, Abbey Tomita, and the taxonomists of the Polish Counting Center for sample enumeration; and we thank Sam Zeman, Anna Bolm, Liv Burnip, Cheryl Morgan, and Amy Wallace for assistance measuring krill. We thank Christopher A. Edwards (University of California) for his help acquiring ROMS data. We thank Brian Wells (NOAA Southwest Fisheries Science Center) for helpful feedback on an earlier version of our manuscript. We thank the two anonymous reviewers who reviewed this work.

Appendix A. Supplementary material

Supplementary data to this article can be found online at https://doi.org/10.1016/j.pocean.2024.103388.

Data availability

Krill layers are available at https://figshare.com/projects/OPAL_Overlap_Predictions_About_Large_whales/161137. Codes are available at https://github.com/SoleneDerville/Krill-distribution-NCC

References

Abraham, C.L., Sydeman, W.J., 2004. Ocean climate, euphausiids and auklet nesting: inter-annual trends and variation in phenology, diet and growth of a planktivorous seabird, Ptychoramphus aleuticus. Mar. Ecol. Prog. Ser. 274, 235–250. https://doi.org/10.3354/meps274235.

Abraham, C.L., Sydeman, W.J., 2006. Prey-switching by Cassin's auklet Ptychoramphus aleuticus reveals seasonal climate-related cycles of Euphausia pacifica and Thysanoessa spinifera. Mar. Ecol. Prog. Ser. 313, 271–283. https://doi.org/10.3354/meps313271.

Abrahms, B., Welch, H., Brodie, S., Jacox, M.G., Becker, E.A., Bograd, S.J., Irvine, L.M., Palacios, D.M., Mate, B.R., Hazen, E.L., 2019. Dynamic ensemble models to predict distributions and anthropogenic risk exposure for highly mobile species. Divers. Distrib. 25, 1182–1193. https://doi.org/10.1111/ddi.12940.

Ainley, D.G., Spear, L.B., Allen, S.G., 1996. Variation in the diet of Cassin's auklet reveals spatial, seasonal, and decadal occurrence patterns of euphausiids off California. USA. Mar. Ecol. Prog. Ser. 137, 1–10. https://doi.org/10.3354/meps137001.

Barlow, D.R., Bernard, K., Escobar-Flores, P., Palacios, D., Torres, L.G., 2020. Links in the trophic chain: modeling functional relationships between in situ oceanography, krill, and blue whale distribution under different oceanographic regimes. Mar. Ecol. Prog. Ser. 642, 207–225. https://doi.org/10.3354/meps13339.

Becker, E.A., Forney, K.A., Redfern, J.V., Barlow, J., Jacox, M.G., Roberts, J.J., Palacios, D.M., 2018. Predicting cetacean abundance and distribution in a changing climate. Divers. Distrib. 25, 626–643. https://doi.org/10.1111/ddi.12867.

Benoit-Bird, K.J., Waluk, C.M., Ryan, J.P., 2019. Forage species swarm in response to coastal upwelling. Geophys. Res. Lett. 46, 1537–1546. https://doi.org/10.1029/2018GL081603.

Bizzarro, J.J., Yoklavich, M.M., Wakefield, W.W., 2017. Diet composition and foraging ecology of U.S. Pacific Coast groundfishes with applications for fisheries management. Environ. Biol. Fishes 100, 375–393. https://doi.org/10.1007/s10641-016-0529-2.

Bliss, L.M., Zamon, J.E., Davoren, G.K., Hanson, M.B., Noren, D.P., Emmons, C., Holt, M. M., 2024. Habitat associations of marine predators in the northern California Current during the low productivity downwelling season. Front. Mar. Sci. 11, 1–16. https://doi.org/10.3389/fmars.2024.1355439.

Bollens, S.M., Frost, B.W., Lin, T.S., 1992. Recruitment, growth, and diel vertical migration of Euphausia pacifica in a temperate fjord. Mar. Biol. 114, 219–228. https://doi.org/10.1007/BF00349522.

Bouchet, P.J., Miller, D.L., Roberts, J.J., Manocci, L., Harris, C.M., Thomas, L., 2019. From Here and Now to There and Then: Practical Recommendations for the Extrapolation of Cetacean Density Surface Models to Novel Conditions. University of St Andrews.

Brinton, E., 1962. The distribution of pacific Euphausiids. Bull. Scripps Inst. Oceanogr. Univ. Calif. 8, 21–270.

Brinton, E., 1967. Vertical migration and avoidance capability of Euphausiids in the California Current. Limnol. Oceanogr. 12, 451–483. https://doi.org/10.4319/lo.1967.12.3.0451.

Brinton, E., Townsend, A., 2003. Decadal variability in abundances of the dominant euphausiid species in southern sectors of the California Current. Deep Res. Part II Top. Stud. Oceanogr. 50, 2449–2472. https://doi.org/10.1016/S0967-0645(03)00126-7.

Brodeur, R.D., Lorz, H.V., Pearcy, W.G., 1987. Food habits and dietary variability of pelagic nekton off oregon. NOAA Tech. Rep. NMFS 57, 1979–1984.

Buckley, T.W., Livingston, P.A., 1997. Geographic variation in the diet of Pacific hake, with a note on cannibalism. Calif. Coop. Ocean. Fish. Investig. Reports 38, 53–62.

Checkley, D.M., Barth, J.A., 2009. Patterns and processes in the California Current system. Prog. Oceanogr. 83, 49–64. https://doi.org/10.1016/j.pocean.2009.07.028.

Chu, E.W., 1984. Sooty Shearwaters off California: diet and energy gain. In: Nettleship, D.N., Sanger, G.A., Springer, P.F. (Eds.), Marine Birds: Their Feeding Ecology and Commercial Fisheries Relationships. Canadian Wildlife Service, Ottawa, Canada, pp. 64–71.

Cimino, M.A., Santora, J.A., Schroeder, I., Sydeman, W., Jacox, M.G., Hazen, E.L., Bograd, S.J., 2020. Essential krill species habitat resolved by seasonal upwelling and ocean circulation models within the large marine ecosystem of the California Current System. Ecography (Cop.) 43, 1536–1549. https://doi.org/10.1111/ecog.05204.

Cragg, J.G., 1971. Some statistical models for limited dependent variables with application to the demand for durable goods. Econometrica 39, 829. https://doi.org/10.2307/1909582.

Croll, D.A., Marinovic, B., Benson, S., Chavez, F.P., Black, N., Ternullo, R., Tershy, B.R., 2005. From wind to whales: trophic links in a coastal upwelling system. Mar. Ecol. Prog. Ser. 289, 117–130. https://doi.org/10.3354/meps289117.

Derville, S., Torres, L.G., Iovan, C., Garrigue, C., 2018. Finding the right fit: comparative cetacean distribution models using multiple data sources and statistical approaches. Divers. Distrib. 24, 1657–1673. https://doi.org/10.1111/ddi.12782.

Derville, S., Barlow, D.R., Hayslip, C.E., Torres, L.G., 2022. Seasonal, annual, and decadal distribution of three rorqual whale species relative to dynamic ocean conditions off Oregon, USA. Front. Mar. Sci. 9, 868566. https://doi.org/10.3389/fmars.2022.868566.

Dorman, J.G., Sydeman, W.J., Bograd, S.J., Powell, T.M., 2015a. An individual-based model of the krill Euphausia pacifica in the California Current. Prog. Oceanogr. 138, 504–520. https://doi.org/10.1016/j.pocean.2015.02.006.

Dorman, J.G., Sydeman, W.J., García-Reyes, M., Zeno, R.A., Santora, J.A., 2015b. Modeling krill aggregations in the central-northern California Current. Mar. Ecol. Prog. Ser. 528, 87–99. https://doi.org/10.3354/meps11253.

Dorman, J.G., Sydeman, W.J., Thompson, S.A., Warren, J.D., Killeen, H.J., Hoover, B.A., Field, J.C., Santora, J.A., 2023. Environmental variability and krill abundance in the central California Current: implications for ecosystem monitoring. Front. Mar. Sci. 10, 1099482. https://doi.org/10.3389/fmars.2023.1099482.

Dormann, C.F., Elith, J., Bacher, S., Buchmann, C., Carl, G., Carré, G., Marquéz, J.R.G., Gruber, B., Lafourcade, B., Leitão, P.J., Münkemüller, T., Mcclean, C., Osborne, P.E., Reineking, B., Schröder, B., Skidmore, A.K., Zurell, D., Lautenbach, S., 2013. Collinearity: a review of methods to deal with it and a simulation study evaluating their performance. Ecography (cop.) 36, 027–046. https://doi.org/10.1111/j.1600-0587.2012.07348.x.

Elith, J., Leathwick, J.R., 2009. Species distribution models: ecological explanation and prediction across space and time. Annu. Rev. Ecol. Evol. Syst. 40, 677–697. https://doi.org/10.1146/annurev.ecolsys.110308.120159.

Emmett, R.L., Brodeur, R.D., Miller, T.W., Pool, S.S., Krutzikowsky, G.K., Bentley, P.J., McCrae, J., 2005. Pacific sardine (Sardinops sagax) abundance, distribution, and ecological relationships in the Pacific Northwest. Calif. Coop. Ocean. Fish. Investig. Reports 46, 122–143.

Endo, Y., 1984. Daytime surface swarming of Euphausia pacifica (Crustacea: Euphausiacea) in the Sanriku coastal waters of northeastern Japan. Mar. Biol. 79, 269–276.

Feinberg, L.R., Shaw, C.T., Peterson, W.T., Décima, M., Okazaki, Y., Ju, S.J., 2013. Euphausia pacifica brood sizes: a North Pacific synthesis. J. Plankton Res. 35, 1192–1206. https://doi.org/10.1093/plankt/fbt064.

Fiechter, J., Santora, J.A., Chavez, F., Northcott, D., Messié, M., 2020. Krill hotspot formation and phenology in the California Current ecosystem. Geophys. Res. Lett. 47, 1–10. https://doi.org/10.1029/2020GL088039.

Fisher, J.L., Menkel, J., Copeman, L., Shaw, C.T., Feinberg, L.R., Peterson, W.T., 2020. Comparison of condition metrics and lipid content between Euphausia pacifica and Thysanoessa spinifera in the northern California Current, USA. Prog. Oceanogr. 188, 102417. https://doi.org/10.1016/j.pocean.2020.102417.

Fleming, A.H., Clark, C.T., Calambokidis, J., Barlow, J., 2016. Humpback whale diets respond to variance in ocean climate and ecosystem conditions in the California Current. Glob. Chang. Biol. 22, 1214–1224. https://doi.org/10.1111/gcb.13171.

Fossette, S., Abrahms, B., Hazen, E.L., Bograd, S.J., Zilliacus, K.M., Calambokidis, J., Burrows, J.A., Goldbogen, J.A., Harvey, J.T., Marinovic, B., Tershy, B., Croll, D.A., 2017. Resource partitioning facilitates coexistence in sympatric cetaceans in the California Current. Ecol. Evol. 7, 9085–9097. https://doi.org/10.1002/ece3.3409.

Friedman, J.H., 2001. Greedy function approximation: a gradient boosting machine. Ann. Stat. 29, 1189–1232, 10.214/aos/1013203451.

Friedman, J., Meulman, J.J., 2003. Multiple additive regression trees with application in epidemiology. Stat. Med. 22, 1365–1381.

Frölicher, T.L., Laufkötter, C., 2018. Emerging risks from marine heat waves. Nat. Commun. 9, 650. https://doi.org/10.1038/s41467-018-03163-6.

Gómez-Gutiérrez, J., Peterson, W.T., Miller, C.B., 2005. Cross-shelf life-stage segregation and community structure of the euphausiids off central Oregon (1970–1972). Deep. Res. Part II Top. Stud. Oceanogr. 52, 289–315. https://doi.org/10.1016/j.dsr2.2004.09.023.

Hand, C.H., Berner, L.J., 1959. Food of the Pacific Sardine. Fish. Bull. Fish Wildl. Serv. 60, 1–14.

Harris, P.T., Macmillan-Lawler, M., Rupp, J., Baker, E.K., 2014. Geomorphology of the oceans. Mar. Geol. 352, 4–24. https://doi.org/10.1016/j.margeo.2014.01.011.

Hastie, T.J., Tibshirani, R.J., 1990. Generalized Additive Models, volume 43 of Monographs on Statistics and Applied Probability. Chapman and Hall/CRC, London.
Hickey, B.M., Banas, N.S., 2008. Why is the northern end of the California Current system so productive? Oceanography 21, 90–107. https://doi.org/10.5670/oceanog.2008.07.
Hill, A.D., Daly, E.A., Brodeur, R.D., 2015. Diet variability of forage fishes in the Northern California Current system. J. Mar. Syst. 146, 121–130. https://doi.org/10.1016/j.jmarsys.2014.08.006.
Kaplan, R.L., Derville, S., Bernard, K.S., Phillips, E.M., Torres, L.G., 2024. Humpback-Krill Relationships are strongest at fine spatial scales in the Northern California Current region. Mar. Ecol. Prog. Ser. 729, 219–232. https://doi.org/10.3354/meps14510.
Killeen, H., Dorman, J., Sydeman, W., Dibble, C., Morgan, S., 2022. Effects of a marine heatwave on adult body length of three numerically dominant krill species in the California Current ecosystem. ICES J. Mar. Sci. 79, 761–774. https://doi.org/10.1093/icesjms/fsab215.
Lee, Y.W., Sampson, D.B., 2009. Dietary variations in three co-occurring rockfish species off the Pacific Northwest during anomalous oceanographic events in 1998 and 1999. Fish. Bull. 107, 510–522.
Marra, G., Wood, S.N., 2011. Practical variable selection for generalized additive models. Comput. Stat. Data Anal. 55, 2372–2387. https://doi.org/10.1016/j.csda.2011.02.004.
Muhling, B.A., Brodie, S., Smith, J.A., Tommasi, D., Gaitan, C.F., Hazen, E.L., Jacox, M. G., Auth, T.D., Brodeur, R.D., 2020. Predictability of species distributions deteriorates under novel environmental conditions in the California Current system. Front. Mar. Sci. 7, 589. https://doi.org/10.3389/fmars.2020.00589.
Neveu, E., Moore, A.M., Edwards, C.A., Fiechter, J., Drake, P., Crawford, W.J., Jacox, M. G., Nuss, E., 2016. An historical analysis of the California Current circulation using ROMS 4D-Var: system configuration and diagnostics. Ocean Model 99, 133–151. https://doi.org/10.1016/j.ocemod.2015.11.012.
Nickels, C.F., Sala, L.M., Ohman, M.D., 2018. The morphology of euphausiid mandibles used to assess selective predation by blue whales in the southern sector of the California Current system. J. Crustac. Biol. 38, 563–573. https://doi.org/10.1093/jcbiol/ruy062.
Oliver, E.C.J., Burrows, M.T., Donat, M.G., Sen Gupta, A., Alexander, L.V., Perkins-Kirkpatrick, S.E., Benthuysen, J.A., Hobday, A.J., Holbrook, N.J., Moore, P.J., Thomsen, M.S., Wernberg, T., Smale, D.A., 2019. Projected marine heatwaves in the 21st century and the potential for ecological impact. Front. Mar. Sci. 6, 1–12. https://doi.org/10.3389/fmars.2019.00734.
Peterson, W.T., Fisher, J.L., Strub, P.T., Du, X., Risien, C., Peterson, J., Shaw, C.T., 2017. The pelagic ecosystem in the Northern California Current off Oregon during the 2014–2016 warm anomalies within the context of the past 20 years. J. Geophys. Res. Ocean. 122, 7267–7290. https://doi.org/10.1002/2017JC012952.
Phillips, E.M., Chu, D., Gauthier, S., Parker-Stetter, S.L., Shelton, A.O., Thomas, R.E., 2022. Spatiotemporal variability of euphausiids in the California Current ecosystem: insights from a recently developed time series. ICES J. Mar. Sci. 79, 1312–1326. https://doi.org/10.1093/icesjms/fsac055.
Phillips, E.M., Malick, M.J., Gauthier, S., Haltuch, M.A., Hunsicker, M.E., Parker-Stetter, S.L., Thomas, R.E., 2023. The influence of temperature on Pacific hake co-occurrence with euphausiids in the California Current ecosystem. Fish. Oceanogr. 32, 267–279. https://doi.org/10.1111/fog.12628.
Qiao, H., Soberón, J., Peterson, A.T., 2015. No silver bullets in correlative ecological niche modelling: insights from testing among many potential algorithms for niche estimation. Methods Ecol. Evol. 6, 1126–1136. https://doi.org/10.1111/2041-210X.12397.
Ratnarajah, L., Abu-Alhaija, R., Atkinson, A., Batten, S., Bax, N.J., Bernard, K.S., Canonico, G., Cornils, A., Everett, J.D., Grigoratou, M., Ishak, N.H.A., Johns, D., Lombard, F., Muxagata, E., Ostle, C., Pitois, S., Richardson, A.J., Schmidt, K., Stemmann, L., Swadling, K.M., Yang, G., Yebra, L., 2023. Monitoring and modelling marine zooplankton in a changing climate. Nat. Commun. 14. https://doi.org/10.1038/s41467-023-36241-5.
Redfern, J.V., Ferguson, M.C., Becker, E.A., Hyrenbach, K.D., Good, C., Barlow, J., Kaschner, K., Baumgartner, M.F., Forney, K.A., Ballance, L.T., Fauchald, P., Halpin, P., Hamazaki, T., Pershing, A.J., Qian, S.S., Read, A., Reilly, S.B., Torres, L. G., Werner, F., 2006. Techniques for cetacean-habitat modeling. Mar. Ecol. Prog. Ser. 310, 271–295. https://doi.org/10.3354/meps310271.
Roberts, D.R., Bahn, V., Ciuti, S., Boyce, M.S., Elith, J., Guillera-Arroita, G., Hauenstein, S., Lahoz-Monfort, J.J., Schröder, B., Thuiller, W., Warton, D.I., Wintle, B.A., Hartig, F., Dormann, C.F., 2017. Cross-validation strategies for data with temporal, spatial, hierarchical or phylogenetic structure. Ecography (Cop.) 40, 913–929. https://doi.org/10.1111/ecog.02881.
Robertson, R.R., Bjorkstedt, E.P., 2020. Climate-driven variability in Euphausia pacifica size distributions off northern California. Prog. Oceanogr. 188. https://doi.org/10.1016/j.pocean.2020.102412.
Robinson, L.M., Elith, J., Hobday, A.J., Pearson, R.G., Kendall, B.E., Possingham, H.P., Richardson, A.J., 2011. Pushing the limits in marine species distribution modelling: lessons from the land present challenges and opportunities. Glob. Ecol. Biogeogr. 20, 789–802. https://doi.org/10.1111/j.1466-8238.2010.00636.x.
Rockwood, R.C., Elliott, M.L., Saenz, B., Nur, N., Jahncke, J., 2020. Modeling predator and prey hotspots: management implications of baleen whale cooccurrence with krill in Central California. PLoS One 15, 1–30. https://doi.org/10.1371/journal.pone.0235603.
Ross, R.M., 1982. Energetics of Euphausia pacifica I. Effects of body carbon and nitrogen and temperature on measured and predicted production. Mar. Biol. 68, 1–13.
Ruzicka, J.J., Brodeur, R.D., Emmett, R.L., Steele, J.H., Zamon, J.E., Morgan, C.A., Thomas, A.C., Wainwright, T.C., 2012. Interannual variability in the Northern California Current food web structure: changes in energy flow pathways and the role of forage fish, euphausiids, and jellyfish. Prog. Oceanogr. 102, 19–41. https://doi.org/10.1016/j.pocean.2012.02.002.
Sabal, M.C., Hazen, E.L., Bograd, S.J., MacFarlane, R.B., Schroeder, I.D., Hayes, S.A., Harding, J.A., Scales, K.L., Miller, P.I., Ammann, A.J., Wells, B.K., 2020. California Current seascape influences juvenile salmon foraging ecology at multiple scales. Mar. Ecol. Prog. Ser. 634, 159–173. https://doi.org/10.3354/meps13185.
Santora, J.A., Sydeman, W.J., Schroeder, I.D., Wells, B.K., Field, J.C., 2011. Mesoscale structure and oceanographic determinants of krill hotspots in the California Current: implications for trophic transfer and conservation. Prog. Oceanogr. 91, 397–409. https://doi.org/10.1016/j.pocean.2011.04.002.
Santora, J.A., Field, J.C., Schroeder, I.D., Sakuma, K.M., Wells, B.K., Sydeman, W.J., 2012. Spatial ecology of krill, micronekton and top predators in the central California Current: implications for defining ecologically important areas. Prog. Oceanogr. 106, 154–174. https://doi.org/10.1016/j.pocean.2012.08.005.
Santora, J.A., Hazen, E.L., Schroeder, I.D., Bograd, S.J., Sakuma, K.M., Field, J.C., 2017. Impacts of ocean climate variability on biodiversity of pelagic forage species in an upwelling ecosystem. Mar. Ecol. Prog. Ser. 580, 205–220. https://doi.org/10.3354/meps12278.
Santora, J.A., Zeno, R., Dorman, J.G., Sydeman, W.J., 2018. Submarine canyons represent an essential habitat network for krill hotspots in a large marine ecosystem. Sci. Rep. 8, 7579. https://doi.org/10.1038/s41598-018-25742-9.
Siegel, V., 2000. Krill (Euphausiacea) life history and aspects of population dynamics. Can. J. Fish. Aquat. Sci. 57, 130–150. https://doi.org/10.1139/cjfas-57-S3-130.
Smith, S.E., Adams, P.B., 1988. Daytime surface swarms of Thysanoessa spinifera (Euphausiacea) in the Gulf of the Farallones. California. Bull. Mar. Sci. 42, 76–84.
Sydeman, W.J., Hobson, K.A., Pyle, P., McLaren, E.B., 1997. Trophic relationships among seabirds in Central California : combined stable isotope and conventional dietary approach. Condor 99, 327–336.
Thayer, J.A., Field, J.C., Sydeman, W.J., 2014. Changes in California Chinook salmon diet over the past 50 years: relevance to the recent population crash. Mar. Ecol. Prog. Ser. 498, 249–261. https://doi.org/10.3354/meps10608.
Tovar-Sanchez, A., Duarte, C.M., Hernández-León, S., Sañudo-Wilhelmy, S.A., 2007. Krill as a central node for iron cycling in the Southern Ocean. Geophys. Res. Lett. 34, 1–4. https://doi.org/10.1029/2006GL029096.
Wood, S.N., 2011. Fast stable restricted maximum likelihood and marginal likelihood estimation of semiparametric generalized linear models. J. R. Stat. Soc. 73, 3–36.
Yates, K.L., Bouchet, P.J., Caley, M.J., Mengersen, K., Randin, C.F., Parnell, S., Fielding, A.H., Bamford, A.J., Ban, S., Barbosa, A.M., Dormann, C.F., Elith, J., Embling, C.B., Ervin, G.N., Fisher, R., Gould, S., Graf, R.F., Gregr, E.J., Halpin, P.N., Heikkinen, R.K., Heinänen, S., Jones, A.R., Krishnakumar, P.K., Lauria, V., Lozano-Montes, H., Mannocci, L., Mellin, C., Mesgaran, M.B., Moreno-Amat, E., Mormede, S., Novaczek, E., Oppel, S., Ortuño Crespo, G., Peterson, A.T., Rapacciuolo, G., Roberts, J.J., Ross, R.E., Scales, K.L., Schoeman, D., Snelgrove, P., Sundblad, G., Thuiller, W., Torres, L.G., Verbruggen, H., Wang, L., Wenger, S., Whittingham, M.J., Zharikov, Y., Zurell, D., Sequeira, A.M.M., 2018. Outstanding challenges in the transferability of ecological models. Trends Ecol. Evol. 33, 790–802. https://doi.org/10.1016/j.tree.2018.08.001.